Collisional energy transfer probabilities of highly excited molecules from KCSI. III. Azulene: $P(E',E)$ and moments of energy transfer for energies up to 40 000 cm^{-1} via self-calibrating experiments

Uwe Hold, Thomas Lenzer, Klaus Luther,[a] and Andrew C. Symonds
Institut für Physikalische Chemie, Universität Göttingen, Tammannstr. 6, D-37077 Göttingen, Germany

Complete experimental transition probability density functions $P(E',E)$ have been determined for collisions between highly vibrationally excited azulene and several bath gases over a wide energy range. This was achieved by applying 2-color "kinetically controlled selective ionization (KCSI)" [U. Hold, T. Lenzer, K. Luther, K. Reihs, and A. C. Symonds, J. Chem. Phys. **112**, 4076 (2000)]. The results are "self-calibrating," i.e., independent of any empirical calibration curve, as usually needed in traditional energy transfer experiments like time-resolved ultraviolet absorption or infrared fluorescence. The complete data set can be described by our recently introduced monoexponential 3-parameter $P(E',E)$ form with a parametric exponent Y in the argument, $P(E',E) \propto \exp[-\{(E-E')/(C_0+C_1 \cdot E)\}^Y]$. For small colliders (helium, argon, xenon, N_2, and CO_2) the $P(E',E)$ show increased amplitudes in the wings compared to a monoexponential form ($Y < 1$). For larger colliders, the wings of $P(E',E)$ have an even smaller amplitude ($Y > 1$) than that provided by a monoexponential. Approximate simulations show that the wings of $P(E',E)$ at amplitudes $< 1 \times 10^{-6}$ (cm^{-1})$^{-1}$ have a nearly negligible influence on the population distributions and the net energy transfer. All optimized $P(E',E)$ representations exhibit a linear energy dependence of the collision parameter $\alpha_1(E) = C_0 + C_1 \cdot E$, which also results in an (approximately) linear dependence of $\langle \Delta E \rangle$ and $\langle \Delta E^2 \rangle^{1/2}$. The energy transfer parameters presented in this study have benchmark character in certainty and accuracy, e.g., with only 2%–5% uncertainty for our $\langle \Delta E \rangle$ data below 25 000 cm^{-1}. Deviations of previously reported first moment data from ultraviolet absorption and infrared fluorescence measurements can be traced back to either the influence of azulene self-collisions or well-known uncertainties in calibration curves. © *2003 American Institute of Physics.* [DOI: 10.1063/1.1622382]

I. INTRODUCTION

Collisional relaxation and activation processes at chemically significant energies play an important role in many molecular reaction systems.[1,2] A complete description is possible if the central quantity governing collisional energy transfer (CET)—the collisional transition probability $P(E',E)$—is known. In the first paper, part I of this series, we presented the details of a method, which can map out complete $P(E',E)$ distributions experimentally, called "kinetically controlled selective ionization (KCSI)."[3] This technique is still the only one available, which allows us to obtain full $P(E',E)$ from relaxing distributions of highly vibrationally excited molecules, even if this donor is characterized by an extremely high, quasicontinuous density of states. From KCSI, the first moment of energy transfer $\langle \Delta E \rangle$ and higher moments, like e.g., $\langle \Delta E^2 \rangle$, and their energy dependence can be extracted with a high degree of accuracy. We have demonstrated this in detail in part II of this series, in which the CET of toluene was investigated up to energies of 50 000 cm^{-1}.[4]

The main body of available experimental CET data however stems from different types of direct experiments, which

detect signals related to the average energy loss in time of a whole population of excited donor molecules in a bath gas M. These methods are sensitive only to the first moment of energy transfer $\langle \Delta E \rangle$, and details on the relaxing population distributions and $P(E',E)$ cannot be obtained. The evaluated $\langle \Delta E \rangle$ results of such studies are heavily dependent on the quality of the calibration curve available, relating the observable (absorption or fluorescence) with the average energy $\langle E \rangle$ of the molecules. By differentiating the $\langle E(t) \rangle$ curve or related methods, the first moment $\langle \Delta E \rangle$ can be obtained.

Over the years, azulene has served as a key system in such experiments, because of its unique photophysical properties (see Sec. II). It was first studied by Barker and co-workers by monitoring its time-resolved infrared fluorescence (IRF) from CH stretching modes during the relaxation process.[5–8] A later reanalysis by the same group with an adjusted calibration curve resulted in a substantial change of the original $\langle \Delta E \rangle$ values by 30%–50%, depending on the bath gas.[9]

On the other hand, several studies employing time-resolved ultraviolet absorption (UVA) have been carried out. The first studies by Hippler and co-workers reported almost energy independent $\langle \Delta E \rangle$ for all colliders, except at the lowest energies.[10] However, later measurements by the same group with an improved signal to noise ratio employing

low[11] and high excitation energies[12] found a more or less linear energy dependence with a potential leveling-off at high energies. The most recent UVA study by Schwarzer and co-workers shows a further improved signal to noise ratio.[13] These experiments were carried out at temperatures $\geqslant 373$ K for excitation energies $<20\,000$ cm^{-1}. They found an essentially linear energy dependence of $\langle \Delta E \rangle$ over the whole energy range, in several cases with substantial deviations from the results of Hippler *et al.*

Because of the considerable spread in $\langle \Delta E \rangle$ between the available experiments (even for the same detection method) and the complete lack of knowledge with respect to $P(E',E)$, there is clearly a need for a high accuracy study of azulene. A thorough investigation of this type is carried out in this paper. We present the first measurements of CET, which are *completely independent* of any calibration curve. This could be achieved, because the information content of the KCSI data set established in this study is so extended that all energy transfer parameters and also the shape of the KCSI observation window function can be deduced from the signals, due to the mathematically very complex character of the sets of the highly correlated KCSI curves.[3,4] From the technical side, we employ for the first time a *2-color* KCSI process and will discuss its implementation in greater detail.

We will show that all our data can be successfully described by our recently introduced monoexponential 3-parameter $P(E',E)$ form with a parametric exponent Y in the argument, $P(E',E) \propto \exp[-\{(E-E')/(C_0+C_1 \cdot E)\}^Y]$. This was originally introduced by us as a purely mathematical function employing a minimum number of parameters. However, very recent theoretical studies by Nordholm and co-workers using a modified statistical model, the ''partially ergodic collision theory (PECT),'' are able to reproduce the shape of the KCSI $P(E',E)$ functions and the observed trends with bath gas size.[14] The PECT study for azulene can be found in the following paper.[65]

II. APPLICATION OF KCSI TO THE AZULENE SYSTEM

A full account of the KCSI technique has already been given in part I of this series,[3] so only the key aspects will be mentioned here. A general KCSI scheme is shown in Fig. 1. Azulene is promoted to an excited electronic state by a pump laser (wavelength λ_0) and undergoes fast internal conversion to produce highly vibrationally excited molecules in the electronic ground state (S_0^*). Subsequently, collisional deactivation in the bath gas M takes place. After a variable delay time t, molecules within a narrowly defined observation window are probed by a 2-color 2-photon KCSI process (wavelengths λ_1 and λ_2), as shown on the right-hand side, via a resonant intermediate state. Two central requirements must be therefore fulfilled for applying KCSI. First, an efficient photophysical process should be available in order to produce a sufficiently large population of highly vibrationally excited molecules. Second, the molecule must posess an electronic intermediate state suitable to provide experimentally useable ''observation windows'' of the KCSI detection process. In both respects, azulene is ideally suited for KCSI studies.
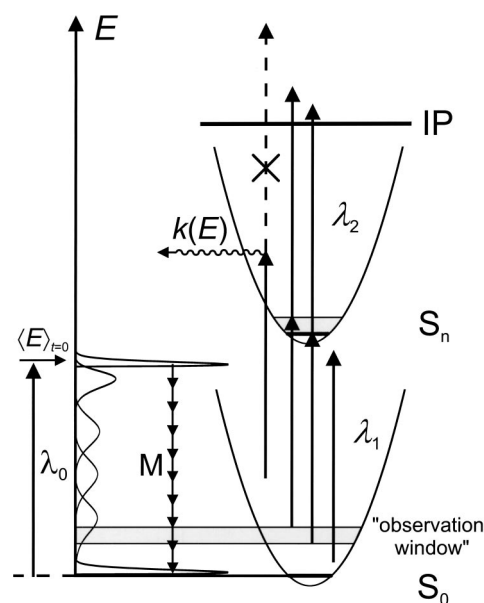

FIG. 1. General scheme for a 1-photon pump 2-photon probe KCSI experiment. Note that the downward arrows on the left side refer to the *net* energy transfer (sum of downward and upward collisions), i.e., $\langle \Delta E \rangle$, which is negative for all energies above $\langle E \rangle = \langle E \rangle_{\text{th}}$ ($=979$ cm^{-1} for azulene at 300 K).

A. Preparation of highly vibrationally excited azulene molecules

We use a fast internal conversion (IC) process for the preparation of a well-defined nascent population of highly vibrationally excited azulene molecules in the electronic ground state: a suitable UV/VIS ns laser pulse is used to promote azulene to an excited electronic state S_n. The subsequent isoenergetic transition $S_n \rightarrow S_0$ is very fast (ns or shorter, see below) compared to the timescale of collisional deactivation (μs). It therefore generates a population of vibrationally hot molecules in S_0^* before any collision occurs. The resulting nascent population distribution can be well described by a thermal Boltzmann distribution at the temperature of the experiment (here 300 K) shifted by the energy of the exciting photon. It is thus very narrow, i.e., quasimicrocanonical, compared to the total energy range of collisional deactivation.

The photophysics of azulene in the gas phase has been studied in considerable detail. The absorption spectrum[15] in Fig. 2 shows several electronic transitions: $S_0 \rightarrow S_1$ (origin 14 283.3 cm^{-1}),[16] $S_0 \rightarrow S_2$ (origin 28 757 cm^{-1}),[17,18] $S_0 \rightarrow S_3$ (origin $\approx 34\,000$ cm^{-1}), $S_0 \rightarrow S_4$ (origin $\approx 36\,000$ cm^{-1}), and $S_0 \rightarrow S_5$ (origin $\approx 42\,000$ cm^{-1}).[19–21] Optical excitation to S_1 results in an efficient, ultrafast internal conversion back to S_0 ($\phi_{\text{IC}} \approx 1$), with a rate constant $k_{\text{IC}} = 1 \times 10^{12}$ s^{-1} at the origin.[22,23] This value was recently questioned by Ruth *et al.*, who find a smaller $k_{\text{IC}} = 3.8 \times 10^{11}$ s^{-1}.[16] k_{IC} increases with increasing excess energy.[16,24] Intersystem crossing ($S_1 \rightarrow T_1$) and fluorescence play no role.[25,26] In the S_2 state, IC is also the dominant process: A quantum yield of $\phi_{\text{IC}} = 0.96$ was found, whereas fluorescence is of minor significance to the present work [$\phi_f(S_2 \rightarrow S_0) = 0.04$ at the origin].[27] The rate constant for
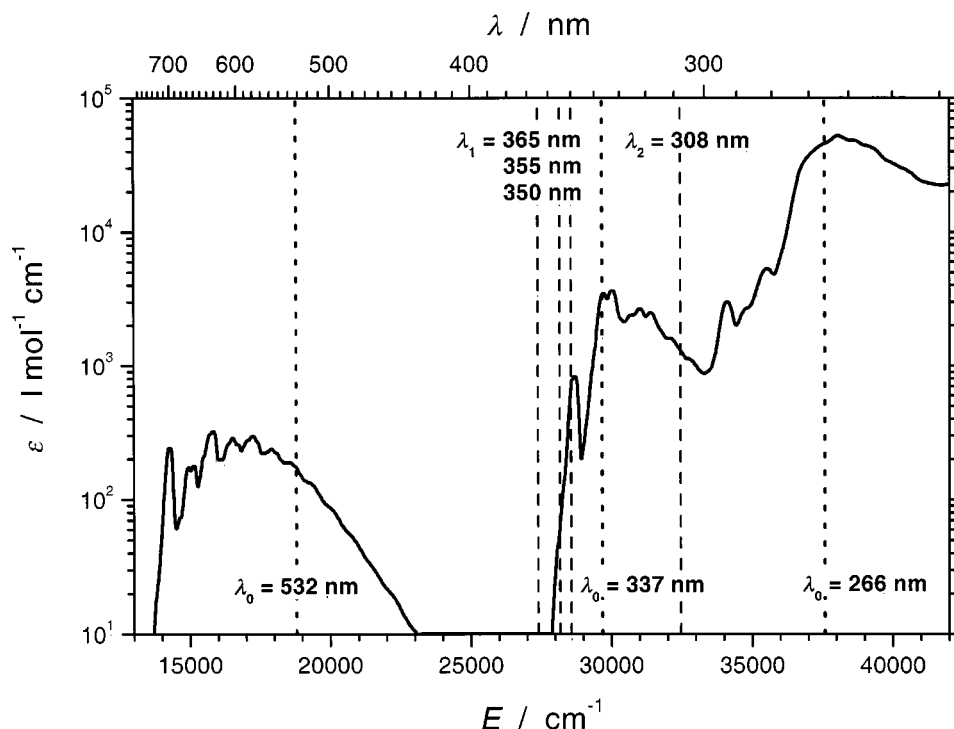
FIG. 2. UV-VIS absorption spectrum of azulene in the gas phase, adopted from Ref. 15. The different KCSI pump and probe wavelengths are shown (pump wavelengths: dotted lines; probe wavelengths: dashed lines).

internal conversion at the origin is $k_{IC} = 2.93 \times 10^8$ s^{-1} and increases with energy.[17,18,27–30] Intersystem crossing from S_2 is negligible.[25] Excitation to the higher electronic states $S_3 - S_5$ also produces highly vibrationally excited S_0^* azulene by IC via the S_2 state.[29,31]

It is therefore clear that azulene is an ideal system to prepare highly vibrationally excited S_0^* molecules, because IC is the dominant process in all its excited electronic states. For the KCSI experiments in this study, we prepared highly vibrationally excited azulene molecules by excitation with $\lambda_0 = 532$ nm (S_1), 337 nm (S_2) or 266 nm (S_4), corresponding to average excitation energies $\langle E \rangle_{th} + hc/\lambda_0$ of 19 776, 30 653 or 38 573 cm^{-1}, respectively, $\langle E \rangle_{th}$ being the average thermal azulene energy at 300 K (979 cm^{-1}).

Finally, the isomerization of azulene to naphthalene has to be considered. The available energy-dependent specific rate constants for this process show that—under the pressure conditions in our study—the isomerization can only compete at very high excitation energies and has no influence on the shape of the KCSI signals,[12,32–34] see Sec. III C for a detailed discussion.

B. "Self-calibrated" and calculated observation windows

As will be discussed in Sec. IV, the information content of the mathematically complex, nonmonotonic KCSI curves of the experiments is so large that the wavelength and energy dependent ionization probabilities (=window functions)[3,4] can be directly obtained from our master equation simulations of the experimental data, see also part I. The energy transfer results of this study are therefore "*self-calibrating*" and no longer dependent on a window function calculated from external molecular data of various accuracy. Nevertheless it is very instructive to compare the self-calibrated win-

dow functions with their calculated counterparts, based on available photophysical data for the azulene system.

The methodology of calculating window functions was already described in part I of this series.[3] Here we focus only on the specific details for azulene. It has been shown that the shape of the window at the wavelength λ_1 and λ_2 depends on the energy dependent rate coefficient $k(E)$ of the loss channels in the resonant intermediate state and the wavelength and energy dependent absorption coefficients in the ground (ϵ_1) and intermediate state (ϵ_2). These three quantities must be determined to be able to calculate the window functions $W(E, \lambda_1, \lambda_2)$ for azulene:

$$W(E(S_0^*), \lambda_1, \lambda_2) = \tfrac{1}{2} \epsilon_1(\lambda_1, E(S_0^*)) \epsilon_2(\lambda_2, E(S_n^*))$$
$$\times [1 + (k(E(S_n^*)) \cdot \tau_{eff})^{4/3}]^{-3/4}. \quad (1)$$

1. Rate constant k(E)

In the case of azulene, S_2 is the ideal candidate for an intermediate state in the KCSI process, because it shows the required pronounced lifetime dependence $\tau(E)$ on excess energy for kinetic control of the ionization process. Very recently, highly accurate lifetime data for about 70 vibrational levels in S_2 up to 3700 cm^{-1} excess energy have become available from fluorescence measurements using time-correlated single photon counting in a molecular beam.[17] It was found that the rate constant $k(=\tau^{-1})$ at the S_2 origin is $k = 2.93 \times 10^8$ s^{-1} and increases with energy. These results confirm and considerably extend the earlier molecular beam measurements of Refs. 27 and 28. In addition, experiments in a gas cell at room temperature also performed in Göttingen yielded precise lifetimes for 20 average excess energies $\langle E \rangle$ between 1900 and 7700 cm^{-1}.[29] In a preliminary analysis, the multiexponential fluorescence decays observed in these thermal experiments were fitted by a monoexponential
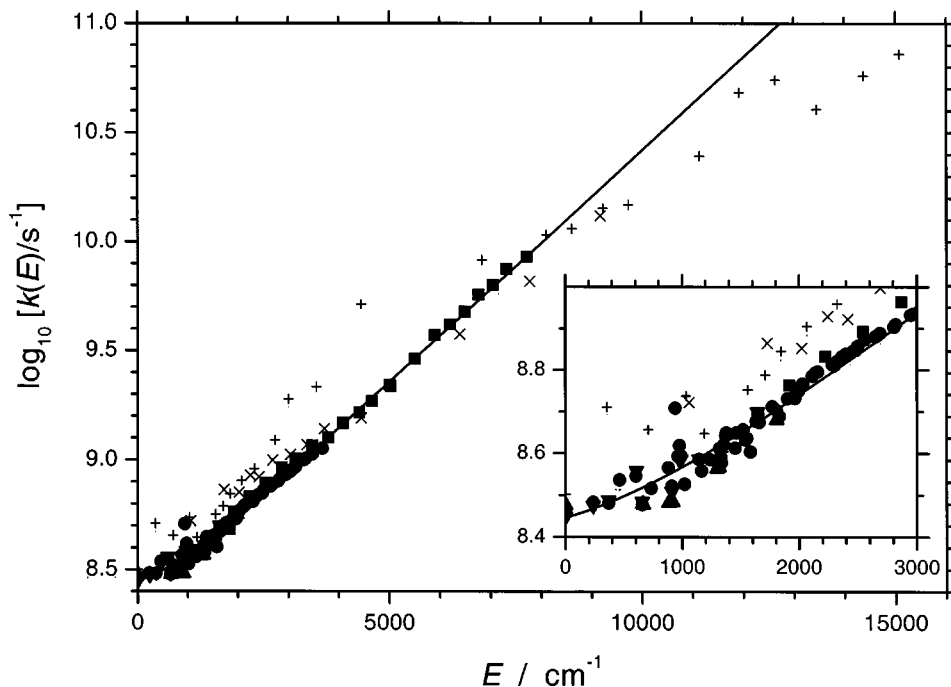
FIG. 3. Rate constant $k(E)$ [=inverse lifetime, $\tau(E)^{-1}$] of the S_2 state decay of azulene. Time-resolved data: ● from Ref. 17, ■ from Ref. 29, ▲ from Ref. 27, and ▼ from Ref. 28. × and + are quantum yield measurements from Refs. 30 and 31, respectively, based on a value of 1×10^7 s^{-1} for the radiative rate constant k_f. The solid line represents a biexponential fit to the time-resolved data [Eq. (2)], which is used for calculating the KCSI windows. The inset shows a magnification for low excess energies in the S_2 state. For details see the text.

function. This yields k values at the average energy $\langle E \rangle$ of the respective thermal distribution, which nicely extend the results of Ref. 17. Note that all time-resolved measurements (shown as filled symbols in Fig. 3), are of very high accuracy, with typical error bars within a point size.

k can also be deduced from the absolute fluorescence emission quantum yields ϕ_f of Amirav for energies up to 15 000 cm^{-1},[31] and relative quantum yields of Hirata et al. given in Ref. 30. Hirata's data were scaled to agree with those of Amirav at low and high energies. Here both data sets are merely included for the sake of completeness. k values deduced from the latter kind of studies are less precise, as they crucially depend on the unknown energy dependent radiative lifetimes. We took a reasonable estimate of 1×10^7 s^{-1} for the radiative rate constant k_f and calculated $k(E)$ from the quantum yield data via $k(E) = k_f / \phi_f(E)$. These values are also included in Fig. 3 (crosses). All time-resolved measurements show excellent agreement. Not un-expectedly, the data of Amirav and Hirata show deviations. For the calculation of $W(E, \lambda_1, \lambda_2)$ we therefore fitted the accurate data points from the time-resolved experi-ments[17,27–29] by a biexponential function (included as a solid line in Fig. 3),

$$\frac{k(E)}{s^{-1}} = 8.42 \times 10^7 \exp\left[-5.1 \times 10^{-4}\left(\frac{E}{\text{cm}^{-1}}\right)\right]$$
$$+ 1.95 \times 10^8 \exp\left[4.9 \times 10^{-4}\left(\frac{E}{\text{cm}^{-1}}\right)\right]. \quad (2)$$

Note that this fit yields very accurate values for $k(E)$ up to energies of 8000 cm^{-1}. This is more than sufficient for calculating the observation window. Uncertainties in $k(E)$ at higher excess energies are irrelevant, because at such energies the window amplitudes are anyway already very small (see below).

2. Absorption coefficients

During the simultaneous irradiation of the relaxing ensemble with the ionizing wavelengths λ_1 and λ_2 it is impossible to distinguish between the two possible absorption sequences

$$S_0^* \xrightarrow{\lambda_1} S_2^* \xrightarrow{\lambda_2} I^+$$

and

$$S_0^* \xrightarrow{\lambda_2} S_2^* \xrightarrow{\lambda_1} I^+ \quad (3)$$
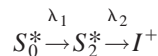
which comprise the ionization process. Therefore it has to be kept in mind that there will be contributions from both combinations. The energy dependence of the ground state absorption for both sequences must be considered. In our earlier investigation on toluene, energy dependent absorption coefficients ϵ_1 were deduced from temperature dependent shock-tube data.[4] Unfortunately, for azulene such experimental results exist only up to wavelengths around 300 nm.[35] However, as the probe wavelengths $\lambda_1 = 365$, 355, and 350 nm used in this study are located on the long wavelength edge of the S_2 band (Fig. 2), we can use a simple exponential Boltzmann expression for describing the temperature dependence of ϵ_1,

$$\epsilon_1(\lambda_1, E(\lambda_1)) = \epsilon_1(\lambda_{\text{ref}}, E(\lambda_{\text{ref}})) \exp\left(-\frac{E(\lambda_{\text{ref}}) - E(\lambda_1)}{k_B T}\right). \quad (4)$$

Here $\epsilon_1(\lambda_{\text{ref}}, E(\lambda_{\text{ref}}))$ is a reference absorption coefficient at a reference wavelength λ_{ref}. In our case we chose ϵ_1 (348 nm, 28 736 cm^{-1})=2750 l mol^{-1} cm^{-1} for $T = 300$ K. For $\lambda_1 = 308$ nm the results of the Sulzer–Wieland treatment in Ref. 32 were interpolated by the expression,
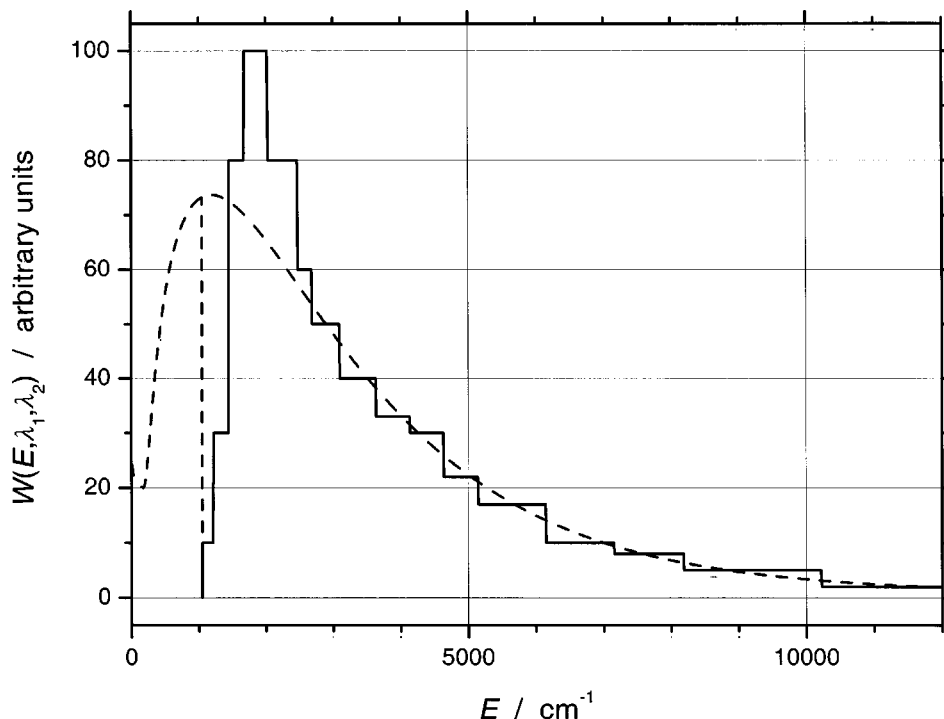
FIG. 4. Optimized KCSI window for $\lambda_1 = 350$ nm from master equation simulations (solid line, histogram) and calculated window for $\lambda_1 = 350$ nm [dashed line, Eq. (1)]. The dashed vertical line marks the cut-off for the optimized window. The amplitudes of both windows have been scaled so that their integral above the cut-off value is identical.

$$\frac{\epsilon_1(308 \text{ nm}, T)}{1 \text{ mol}^{-1} \text{ cm}^{-1}} = 1610 - 0.031\left(\frac{T}{K}\right) + 1.57 \times 10^{-3}\left(\frac{T}{K}\right)^2, \tag{5}$$

which is valid in the range 300–2700 K. The transformation between T and $\langle E \rangle$ in azulene can be accomplished via the partition function

$$\langle E \rangle = \sum_{i=1}^{48} \left[h\nu_i \Big/ \left(\exp\left(\frac{h\nu_i}{k_B T}\right) - 1 \right) \right] \tag{6}$$

using the 48 experimental vibrational frequencies ν_i for azulene.[36] Between 300 and 2000 K this relationship can be well described by the expression,

$$\frac{T}{K} = 289 \times \log_{10}\left(\frac{\langle E \rangle}{\text{cm}^{-1}}\right) + 0.03014\left(\frac{\langle E \rangle}{\text{cm}^{-1}}\right) - 620. \tag{7}$$

As discussed in our earlier publication, the absorption coefficient from higher lying vibrational levels of electronically excited azulene states, $\epsilon_2(\lambda_2, E(S_2^*))$, into the ionization continuum (vertical ionization potential for azulene, 59 781 cm^{-1}) (Ref. 37) should be to a good approximation energy independent.[4] This is supported by a very recent comparison[38] of the fluorescence excitation[39–41] and 1-color (1+1) REMPI spectra[38] for the $S_0 \rightarrow S_1$ transition of *trans*-stilbene in a molecular beam. In both types of experiments very similar spectral line intensities are found. The absorption coefficient for the second step in the REMPI process therefore appears to be virtually constant (i.e., independent of the S_1 vibrational level prepared) and largely independent of the specific wavelength λ_2 for the transition from S_1 into the ionization continuum.

3. $W(E, \lambda_1, \lambda_2)$ from independent molecular data and from master equation simulations

By combining the expressions for $k(E)$ and ϵ_1 [Eqs. (2), (4), and (5)] with Eq. (1) and assuming a constant value for ϵ_2, "window functions for each wavelength λ_1" (i.e., the summed ionization probabilities of the two contributions $\lambda_1 + \lambda_2$ and $\lambda_2 + \lambda_1$, where λ_2 is always 308 nm) can be calculated. At this point it is possible to confront these windows with our optimized ionization probabilities as obtained from our master equation simulations. In Fig. 4 a comparison between the optimized windows (solid line) and the ones determined from independent molecular data (dashed line) is shown for $\lambda_1 = 350$ nm.

First, we compare the decay of the window functions at energies above roughly 2000 cm^{-1}. This is due to the strong decrease of the lifetime [=increase of $k(E)$] in the S_2 state with increasing excess energies which gradually closes the window towards high energies. We find satisfactory agreement between the optimized window function (which automatically came out from our master equation simulations) and the calculated one. This is nice experimental evidence that our method to calculate window functions is essentially correct and reliable, especially with respect to systems where the experimental data set is not as complete as for azulene.

Deviations between the self-calibrated and calculated window are visible at the low energy edge. The former one has its lower edge at higher energies. Such a higher cut-off of the optimized windows relative to the windows calculated from independent molecular data has been also observed for toluene.[4] As explained in detail in our earlier publication, this difference is due to the continuous description of the window function which of course does not take into account quantization effects at the lowest energies: Sparser structures of rovibrational levels show up at sufficiently low energies of

the electronic intermediate state and become especially important for relaxed molecules at energies close to the ground state even for larger polyatomic molecules like azulene. As a result, the *a priori* ''windows'' calculated from external molecular parameters will overestimate the effective ionization coefficient at their low energy edge. Truncating the low end of such windows provided a surprisingly effective ad hoc correction for the neglected quantum effects at least for sufficiently large molecules.[4] After truncation, an identical decay behavior at higher energies is obtained when both types of windows are scaled to have the same integral (as done in Fig. 4). Such a normalization procedure is reasonable, because it ensures that both windows generate (approximately) the same absolute signal *amplitude*. Note that the introduction of such a normalization factor has no influence on the *shape* of the KCSI fit. It should also be mentioned that there is no way to conclude from some visible ambiguities between alternative observation windows (e.g., in Fig. 4) on possibly resulting uncertainties of corresponding KCSI results without detailed modeling. We refer to a long section, IV B of part II,[4] where it has been discussed in detail and shown quantitatively that there is only a surprisingly low influence of shape and extension of the lower part of the window on the KCSI data and thus the derived values.

III. EXPERIMENTAL DETAILS

A. Overview of the setup

Full details of the KCSI setup were already discussed in Ref. 3 so only the specifics for azulene will be given here. The pump wavelength λ_0 (532, 337 or 266 nm) was typically produced by an excimer pumped dye-laser (with optional frequency doubler for 266 nm). For some measurements a frequency-doubled or quadrupled Nd:YAG laser was used (532 and 266 nm). The tunable probe wavelength λ_1 (350, 355, and 365 nm) was generated by a similar excimer/dye laser combination. A small portion of the excimer beam was split off and used as wavelength λ_2. Typical fluences were 8–12 mJ cm^{-2} for the pump beam (diameter $d_0 \geq 2.5$ mm) and 30–45 mJ cm^{-2} for the dye laser beam (diameter d_1 ≥ 1.5–2.0 mm). In contrast, the excimer laser output was strongly attenuated, which led to a considerable improvement in signal quality (fluence typically 0.2 mJ cm^{-2}, d_2 $= d_1$). Signals at 266 nm excitation had a much higher background of ions produced by the pump laser and consequently worse quality. Therefore only selected signals for helium and argon were measured.

Bath gas pressures in the flow system ranged from about 6 mbar (He) to roughly 0.6 mbar (*n*-heptane), corresponding to a typical pump–probe delay of 5–10 μs. The partial pressure of azulene in the cell was extremely low so that azulene self-collisions had no influence on the measured KCSI curves. This was routinely checked by changing the ratios of the partial pressures. No changes in the signal shape were observed.

The chemical substances were all commercially available: azulene from Aldrich (>99%), helium, argon, N$_2$ and CO$_2$ from Messer-Griesheim (all better than 99.995%), xenon from Linde (99.990%); 1,3,5-cycloheptatriene (CHT)
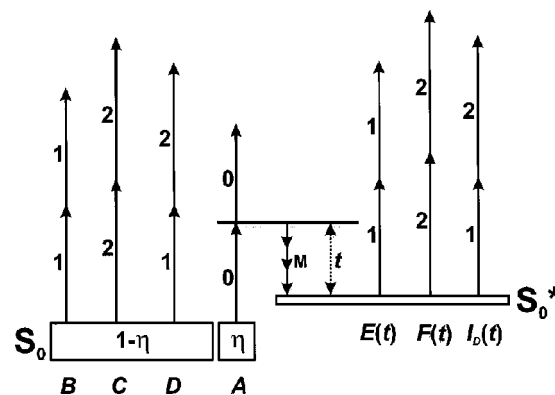

FIG. 5. The possible ionization channels in a three-color $(\lambda_0, \lambda_1, \lambda_2)$ KCSI experiment. The numbers refer to the wavelength indices. $A - I_D(t)$ represent the ion yields from the individual ionization channels shown and η is the total degree of excitation. ''M'' together with the sequence of downward arrows denote the deactivation by the bath gas during the time delay t between the pump and probe pulses.

from Fluka (>95%); *cis*-2-butene (>95%) and *n*-heptane (>99%) from Merck. Azulene was stored in the dark and further purified by vacuum sublimation directly before use. The CHT samples were carefully distilled to remove residual impurities and stored in the dark at 253 K. All liquid colliders were thoroughly degassed by several freeze–pump–thaw cycles before use.

B. Isolating the two-color 1+1 KCSI ion signal

In a multicolor REMPI pump–probe experiment of the present type it is essential to have an unambiguous method for extracting the ion signal of interest from the sum total of all participating ionization channels. Figure 5 presents all the possible channels in such a 3-color pump–probe experiment. Measurement of the time-dependent KCSI signal $I_D(t)$ (the 2-color, 2-photon ionization of the relaxing vibrationally excited population) will be unavoidably accompanied by the simultaneous registration of the ion signals $A - F$. The time-dependent total ion signal registered $I_{\text{tot}}(t)$ is given by

$$I_{\text{tot}}(t) = A + (1-\eta)B + (1-\eta)C + (1-\eta)D + E(t)$$
$$+ F(t) + I_D(t), \qquad (8)$$

where η is the total degree of excitation. In order then to extract $I_D(t)$ from $I_{\text{tot}}(t)$, η and each of the ion signals $A - F$ must be quantified. To this end, separate control measurements were performed throughout the experiment, which monitored the various ion channels. The six control measurements and their associated ion channels are presented in Table I. Like $I_{\text{tot}}(t)$, the ion signals $E(t)$ and $F(t)$ involve ionization of the vibrationally excited azulene population during collisional relaxation. They are therefore time-dependent and were remeasured at each new delay setting. Channels $A - D$, whilst not delay-dependent, were nevertheless regularly monitored throughout the experiment to avoid long-term drifting in the laser energies.

Since the control measurements $I_0 - I_5$ and the measurement of the total ion signal $I_{\text{tot}}(t)$ are not simultaneous, and as minor variations in the experimental conditions are inevitable, precautions had to be taken to ensure that the control

TABLE I. The measurements performed in a 1-color-pump-2-color-probe KCSI experiment. I_0-I_5 are control measurements, whereas $I_{tot}(t)$ is the time-dependent total ion signal. t is the time delay between the pump pulse λ_0 and the probe pulses λ_1 and λ_2.

Measured ion signals	Wavelengths employed			Participating ion channels
I_0	λ_0	$\cdots$	$\cdots$	A
I_1	$\cdots$	λ_1	$\cdots$	B
I_2	$\cdots$	$\cdots$	λ_2	C
I_3	$\cdots$	λ_1	λ_2	$B+C+D$
$I_4(t)$	λ_0	λ_1	$\cdots$	$A+(1-\eta)B+E(t)$
$I_5(t)$	λ_0	$\cdots$	λ_2	$A+(1-\eta)C+F(t)$
$I_{tot}(t)$	λ_0	λ_1	λ_2	$A+(1-\eta)(B+C+D)+E(t)+F(t)+I_D(t)$

ion signals recorded remained relevant for the measurement of $I_{tot}(t)$: Reasonably stable temperature conditions and preliminary flow times long enough to ensure attainment of steady-state conditions resulted in only very slight pressure variations throughout the experiment, implying insignificant changes in the azulene concentration of the highly diluted gas mixture. Long-term drifting in the laser energies was compensated for by discriminating against energies more than about 5% above or below the mean beam energies as measured at the start of the experiment. The effectiveness of this procedure was monitored by the constancy of reference I_{tot} signals measured regularly throughout the experiment at a chosen fixed delay time t_{ref}. The reference signals also served to check for the effects of any loss in cell window transmission due to slowly accumulating deposits of photoproducts, though this was rarely a problem at the fairly low laser intensities employed. The resulting variation in the reference measurements was found to be so small that neither the subsequent normalization of the signal amplitudes to an appropriate reference energy, nor their correction as a function of the running total of laser shots, was necessary.

Shot-to-shot variations in the laser energies are inevitable and lead to corresponding variations in the ion signals which, assuming unsaturated transitions, scale with the power of the number of photons involved in the ionizing transition. In order to compensate for the effects of such energy fluctuations, the following expressions were adopted to describe the observed energy dependences of the control measurement ion signals I_0-I_5, for control measurements I_0-I_2,

$$I_c = k_c E_i^{m_{c,i}} \qquad (9)$$

and for control measurements I_3-I_5,

$$I_c = k_c E_i^{m_{c,i}} E_j^{m_{c,j}}, \qquad (10)$$

where c is the number of the respective control measurement ($c = 0-5$), E_i is the beam energy of laser i, and k_c and $m_{c,i}$ the corresponding fit parameters describing the observed energy dependence of I_c on E_i. Those control measurements which were known to produce no ions (e.g., I_0 with $\lambda_0 = 532$ nm) were not recorded. All others involved recording the ion signal and the laser energies over typically 15–50 laser shots. Subsequent least-squares minimization of the linearized forms of Eqs. (9) and (10) enabled the fit parameters
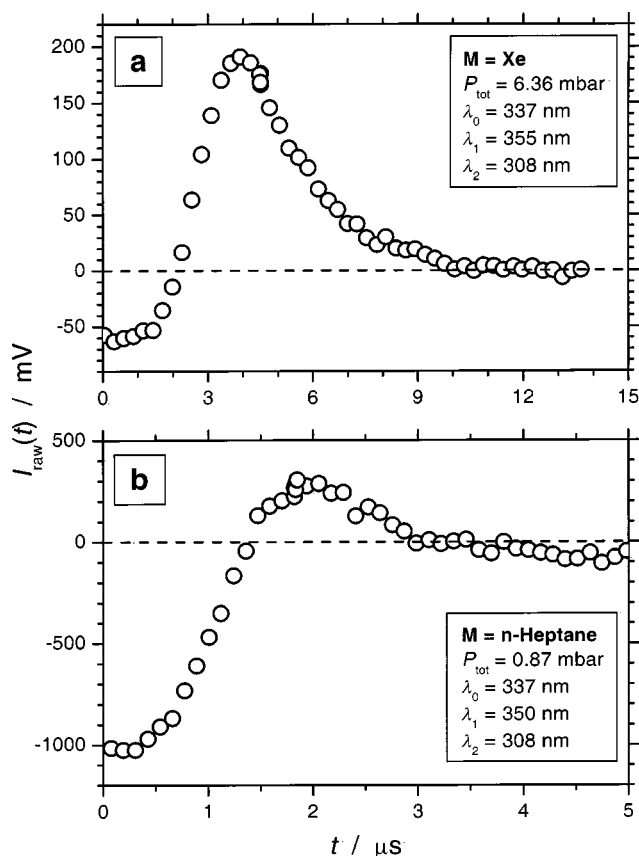

FIG. 6. Signals of single KCSI measurements for the deactivation of highly vibrationally excited azulene. The absolute ion yield of the KCSI process is shown as a function of the delay time t between the pump and probe lasers. (a) M=xenon, pump: $\lambda_0 = 337$ nm, probe: $\lambda_1/\lambda_2 = 355$ nm/308 nm, $P = 6.36$ mbar; (b) M=n-heptane, pump: $\lambda_0 = 337$ nm, probe: $\lambda_1/\lambda_2 = 350$ nm/308 nm, $P = 0.87$ mbar. Note the slightly negative final offset at $t = 5$ μs for the signal in (b).

k_c and $m_{c,i}$ to be determined. For each of the 50 shots which made up a single determination of $I_{tot}(t)$, the beam energies and the appropriate fit parameters from the corresponding control measurements were combined to determine the ion signals I_0-I_5. The ion signals $A-F$ were then taken into account by calculating a "raw" difference signal $I_{raw}(t)$,

$$I_{raw}(t) = I_{tot}(t) + I_0 + I_1 + I_2 - I_3 - I_4(t) - I_5(t). \qquad (11)$$

Substituting the expressions from Eq. (8) and Table I gives

$$I_{raw}(t) = I_D(t) - \eta D, \qquad (12)$$

which provides access to the KCSI signal $I_D(t)$ given that η and D are known.

If the ion signal D is nonzero, i.e., if the ionization window does not lie energetically above the fully relaxed thermal vibrational distribution, and given that η is not negligibly small, the "raw" ion signal will have a negative initial offset and a final value of zero. An example of such a single experimental KCSI curve for the collider xenon is shown in Fig. 6(a). The initial negative offset in $I_{raw}(t)$ arises because immediately following preparation ($t = 0$), no part of the relaxing population has yet reached the ionization window [i.e., $I_D(t=0)=0$]. At long times, the KCSI ion signal $I_D(t)$ from the then fully relaxed population will be simply ηD

and therefore $I_{\text{raw}}(t\rightarrow\infty)=0$. Since the ion signal D is calculable from the control measurements (Table I) and ηD is available from $I_{\text{raw}}(t=0)$, one has direct experimental access to the total degree of excitation η via

$$\eta=-\frac{I_{\text{raw}}(t=0)}{D}=-\frac{I_{\text{raw}}(t=0)}{I_3-I_2-I_1}. \tag{13}$$

For the curve in Fig. 6(a) using $D=641$ mV and $I_{\text{raw}}(t=0)=-62$ mV one obtains a total degree of excitation of $\eta=9.7\%$.

We want to conclude this paragraph with a few remarks on the error limits in our azulene KCSI measurements. The time-delay between the pump and probe pulses can be measured with high accuracy. With an upper limit for the time measurement error of 1 ns, we obtain—at a typical maximum position of a KCSI signal ($\Delta t=2000$ ns)—a negligible error of 0.05%. The pressure measurement is precise within roughly 0.3%, so the uncertainty on the "number of collision axis" $Z_{\text{LJ}}[\text{M}]t$ (see below) is less than 0.4%. The uncertainty of the measured KCSI ion yield is more difficult to estimate. For each time delay the total ion yield and control measurements were typically averaged over 15–50 laser shots, and then the aforementioned subtraction scheme was applied. Several of these KCSI signals were then averaged. We estimate a 1%–4% uncertainty in the ion signal (compare, e.g., the tail regions of the signals in Fig. 6). Further assessment of upper and lower error limits on the basis of the master equation analysis in Sec. IV C yields uncertainties in the moments of energy transfers of about 2%–5%, in reasonable agreement with the values obtained in this section.

C. Influence of multiphoton processes and the isomerization to naphthalene

At higher pump laser powers, the total degree of excitation rises, apparent as a larger initial negative offset $I_{\text{raw}}(t=0)$, but also the fraction of 2- or multi-photon absorption increases, populating higher lying electronic states. As already described in Sec. II A, rapid internal conversion is the dominant decay channel from these states, which produces highly vibrationally excited S_0 azulene via the S_2 state. The multiphoton absorption of λ_0 would lead to a multimodal distribution of highly vibrationally excited ground state azulene. In the following, we denote the excited ground state population resulting from 1-photon absorption and subsequent efficient IC as S_0^*, that following 2-photon excitation as S_0^{**}, etc.

Several influences can be expected: Higher pump intensities will give rise to improved signal to noise ratios due to the increased fraction of molecules excited. In addition, the signal will rise later and be broader than its counterpart recorded at lower pump energies. Such a behavior has been indeed observed in our measurements for azulene pumped at $\lambda_0=532$ nm (not shown here). Qualitatively, this dependence of the signal shape on the laser pump intensity can be easily accounted for by the fact that the S_0^{**} populations require a longer collisional deactivation period before reaching the ionization window. A quantitative interpretation of such a KCSI signal, however is very difficult, as it would require a detailed knowledge on the various (not known) absorption

coefficients of the S_0^*, S_0^{**},... populations to reliably model their individual contributions. For this reason, extreme care was taken in the measurements at the excitation wavelength $\lambda_0=532$ nm. The pump laser intensity was attenuated to a level low enough to prevent visible influences of multiphoton excitation on the KCSI signal.

Interestingly, such a dependence of signal shape on pump laser intensity was not observed for $\lambda_0=337$ nm, and this is indicative of a further process which has to be considered, the isomerization to naphthalene. If the S_0^*, S_0^{**}, S_0^{***},... populations undergo efficient, rapid unimolecular reaction to "inert" products, they are effectively removed, leaving only the S_0^* population which then collisionally relaxes. The resulting KCSI signal should thus be identical in shape (though not in absolute amplitude) to that recorded at lower pump laser intensities (where only the S_0^* population is produced). We have found evidence for such a mechanism, as demonstrated in Fig. 6(b) for the collider n-heptane as an example. The raw KCSI signal has both an initial and final negative offset. This can be easily explained as follows: The value of I_D from the fully relaxed population is $I_D(t\rightarrow\infty)=\eta_{1-P}D$, where η_{1-P} is the degree of single-photon excitation. With η being the total degree of excitation (i.e., 1- plus multiphoton) as above, one has $I_{\text{raw}}(t=0)=-\eta D$. As $\eta_{1-P}<\eta$, one predicts a negative raw ion signal at long times, i.e., $I_{\text{raw}}(t\rightarrow\infty)=(\eta_{1-P}-\eta)D$. For the specific example in Fig. 6(b) [$D=5395$ mV and $I_{\text{raw}}(t=0)=-1035$ mV] one obtains a total degree of excitation $\eta=19.2\%$ with a 1-photon contribution $\eta_{1-P}=17.6\%$. Thus the multiphoton contributions amount to a total of 1.6%.

The observed behavior is also in excellent accord with the known energy dependence of the rate coefficient $k(E)$ for the isomerization azulene$\rightarrow$naphthalene.[12,32–34] The isomerization yield in such a photoactivated system can be estimated from the Stern–Volmer expression,

$$\phi_{\text{iso}}=\frac{\langle k_{\text{iso}}(E_{\text{ac}})\rangle}{\langle k_{\text{iso}}(E_{\text{ac}})\rangle+\gamma_C Z_{\text{LJ}}[\text{M}]}, \tag{14}$$

where E_{ac} is the mean initial energy of the various vibrationally excited ground state populations S_0^*, S_0^{**},..., and $\langle k_{\text{iso}}(E_{\text{ac}})\rangle$ is taken from the fit in Ref. 12. The calculation is detailed here for the collider gas He. [Analogous calculations for heavier bath gas species (γ_C higher, [M] lower) lead to identical conclusions.] Z_{LJ} is given in Table II, and the helium pressure was 6 mbar. Finally, the collisional efficiency γ_C was calculated using the analytical formula of Troe,[42]

$$\frac{\gamma_C}{1-\gamma_C^2}\approx\frac{-\langle\Delta E\rangle s^*}{E-E_0}. \tag{15}$$

The values for the parameters s^* and E_0 were taken from Ref. 32, and approximate $\langle\Delta E\rangle$ from Ref. 11. The resulting isomerization yields are presented in Table III. The expected trends based upon the above arguments are confirmed. Pumping with $\lambda_0=532$ nm produces effectively no naphthalene except at the highest pumping powers when 3-photon absorption may be relevant. If pump laser intensities high enough to produce significant quantities of S_0^{**} are

TABLE II. Lennard-Jones collision numbers and potential parameters for collisions between azulene and the collider gas M (CHT=1,3,5-cycloheptatriene).

M	σ_M (Å)	ϵ_M/k_B (K)	Z_{LJ} (10^7 mbar^{-1} s^{-1})	Z_{LJ} (10^{-10} cm^3 s^{-1})
azulene	6.61	523	⋯	⋯
He	2.55	10.22	1.971	8.108
Ar	3.47	113.5	1.272	5.233
Xe	4.05	230	1.167	4.800
N_2	3.74	82.0	1.433	5.895
CO_2	3.94	201	1.552	6.383
cis-2-butene	5.27	312	2.026	8.334
CHT	5.83	423	2.053	8.448
n-heptane	6.65	351	2.169	8.923

employed, the result will be broadened signals whose analysis is not straightforward due to the difficulty in characterizing the initial multimodal vibrational distribution. For this reason, the $\lambda_0 = 532$ nm signals were recorded at intensities low enough to prevent significant amounts of multiphoton absorption. The situation for $\lambda_0 = 337$ nm is very different, where 2- and multiphoton excitation initiates efficient ($\phi_{iso} \approx 1$) isomerization to naphthalene. Since naphthalene is transparent at the wavelengths employed in the present work, the KCSI ion signals will not be disturbed by its production. The $\lambda_0 = 337$ nm signals could thus be recorded at significantly higher laser intensities than the $\lambda_0 = 532$ nm signals, with the increased fraction of S_0^* resulting in an improved signal to noise ratio.

IV. KCSI CURVES AND QUANTITATIVE ANALYSIS OF $P(E',E)$

Our azulene KCSI measurements can be found in Figs. 7–14 together with optimized fits from a master equation analysis (see below). The results for the pump wavelength $\lambda_0 = 266$ nm have been omitted for the sake of clarity. Each signal represents the average of between four and eight separate experiments, and is shown, normalized to its maximum, as a function of the average number of collisions $Z_{LJ}[M]t$, experienced at time t. Note that putting the KCSI data on a number of collision scale is only a matter of convenience for comparison with older data. This procedure is totally equivalent with discussing CET rates. For a summary of the Lennard-Jones collisions numbers Z_{LJ} in this study (including effective well depths ϵ_{LJ} and radii σ_{LJ}), see Table II.

TABLE III. Estimated isomerization yields for single- and multiphoton excited ground state azulene populations in 6 mbar helium.

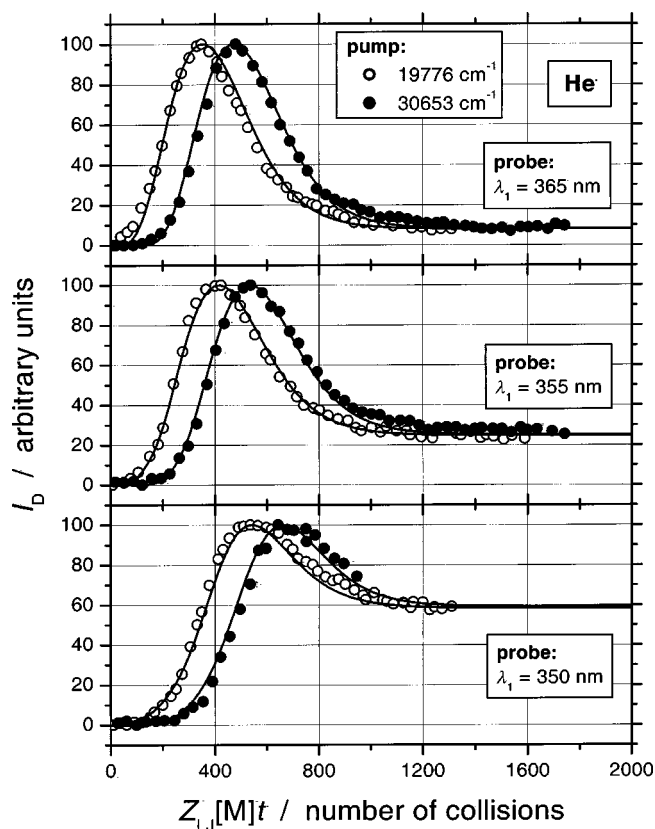| λ_0 (nm)	Number of photons absorbed	E_{ac} (cm^{-1})	$k_{iso}(E_{ac})$ (s^{-1})	γ_C	Φ_{iso}
	1	19 776	below threshold	⋯	0
532	2	38 573	1×10^4	0.039	<0.01
	3	57 370	6×10^6	0.018	0.74
	1	30 653	1×10^2	0.085	≪0.01
337	2	60 326	1×10^7	0.019	0.82
	3	90 000	5×10^8	0.011	>0.99

FIG. 7. KCSI data for the deactivation of highly vibrationally excited azulene by helium. Two different excitation energies (○, 19 776 cm^{-1}; ●, 30 653 cm^{-1}, measurements for 38 573 cm^{-1} not shown here for the sake of clarity) and three different observation windows ($\lambda_1 = 365$, 355, and 350 nm). The lines represent an optimized fit obtained from a master equation analysis using a monoexponential transition probability with parametric exponent Y in the argument [Eq. (16) and Table IV].

They were calculated as described in Ref. 43. Missing data for ϵ_{LJ} and σ_{LJ} of individual substances were determined either from critical data or on basis of a reference substance (e.g., naphthalene in the case of azulene) by using increment tables for structural groups.[44]

The lines in each figure represent our best master equation fit using a monoexponential transition probability function $P(E',E)$ with parametric exponent in the argument [Eq. (16), see below]. The KCSI curves show the same systematic trends as in our toluene measurements:[4] with decreasing probe wavelength (from top to bottom) the observation windows are shifted down the energy scale. Consequently, the corresponding KCSI signals for an excitation energy of 19 776 cm^{-1} appear at increasingly later times (the population distribution needs more collisions to reach the window). At the same time, the residual ion signal increases due to the larger overlap between the window and the Boltzmann distribution. KCSI signals for increasingly higher excitation energies (30 653 cm^{-1} and 38 573 cm^{-1}) show exactly the same trends. They are, however, systematically shifted to larger number of collisions, as the population distribution needs more collisions to reach the respective window. Note that—for a given window—the difference in "arrival times" between two excitation energies is an approximate direct measure of $\langle \Delta E \rangle$ in this energy interval. For instance, in Fig. 7 (helium) a difference of roughly 120 collisions (easily
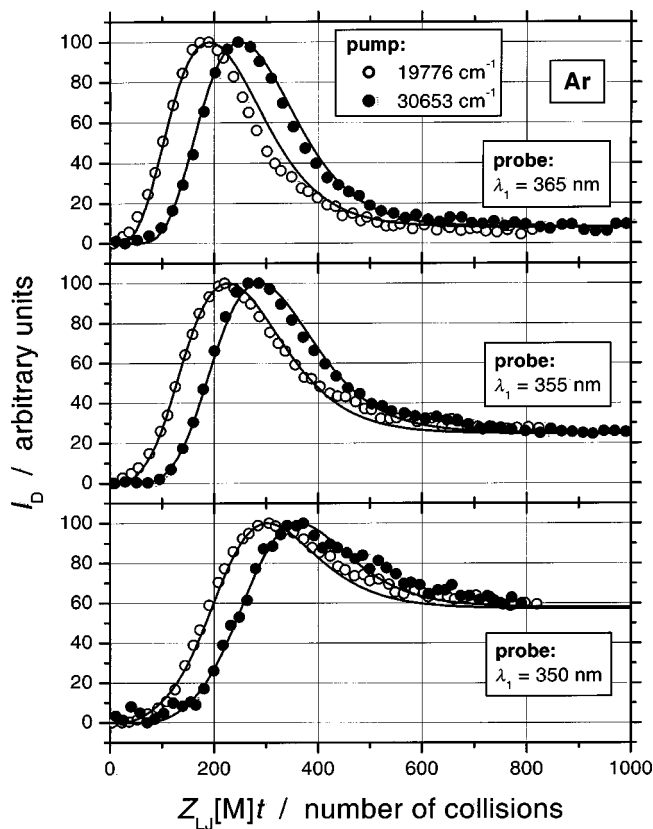
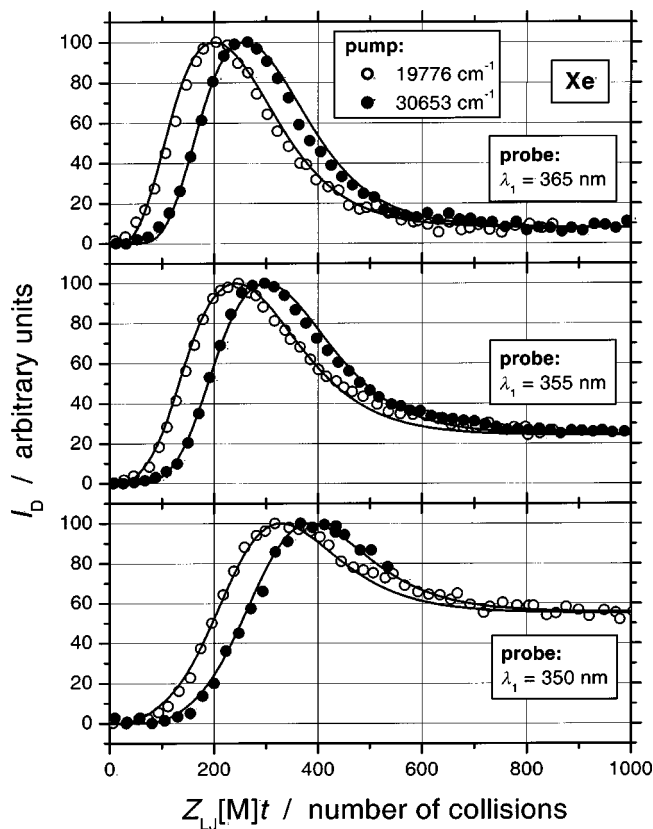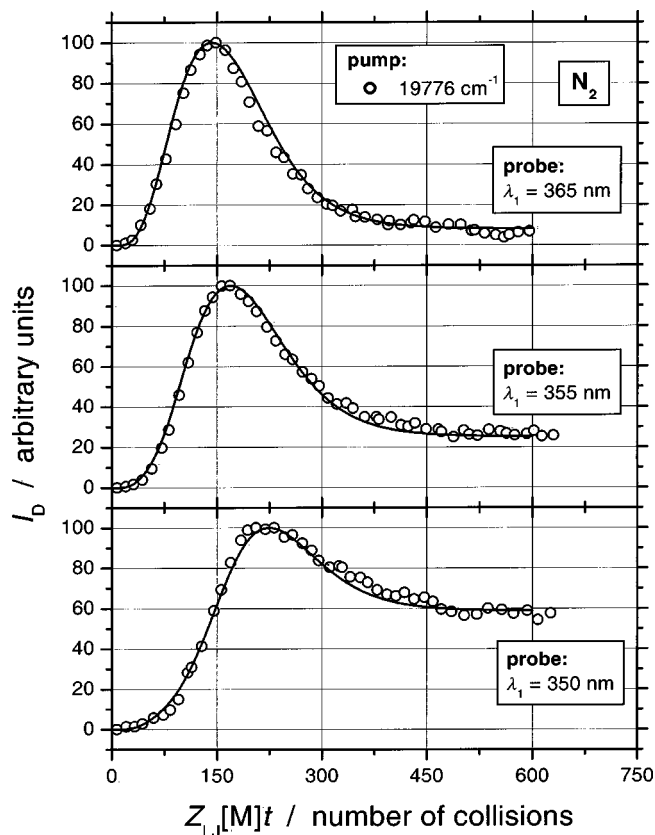FIG. 8. Same as in Fig. 7, but for the collider argon.

FIG. 10. Same as in Fig. 7, but for the collider N_2. Only measurements at the excitation energy 19 776 cm^{-1} are available for this bath gas.

FIG. 9. Same as in Fig. 7, but for the collider xenon.

measured with ruler and pencil) for excitation at 30 653 cm^{-1} and 19 776 cm^{-1}, gives an average $\langle\Delta E\rangle$ of -91 cm^{-1} from a simple back-of-the-envelope calculation, in excellent agreement with the exact result of the detailed master equation analysis (see Fig. 18 below) presented in the following.

A. Best fit $P(E',E)$: Monoexponential with parametric exponent Y

As in our earlier publications, we employed a master equation approach to explore the full information content of the KCSI curves.[3,4] Experimental vibrational frequencies from Ref. 36 were used to calculate the densities of states of azulene using the Whitten–Rabinovitch approximation. A grain size of 20 cm^{-1} was employed in all simulations.

Because in the present case the experimental information basis for azulene from mathematically complex and highly correlated KCSI curves is so extensive (three excitation wavelengths, three detection windows and eight bath gases), no assumptions with respect to the window functions have to be made. In other words, both, the actually used KCSI windows and the $P(E',E)$ parameters, can be extracted in a unique way from our fits to the KCSI data. This is a major step forward compared to traditional energy transfer methods, which always have to rely on the validity of some external calibration input.[9,11]

Just as in the case of toluene CET, our recently introduced functional form of $P(E',E)$ (monoexponential with a parametric exponent Y in the argument), provides an optimum representation for all azulene–bath gas combinations studied.[45] For downward collisions it is given by
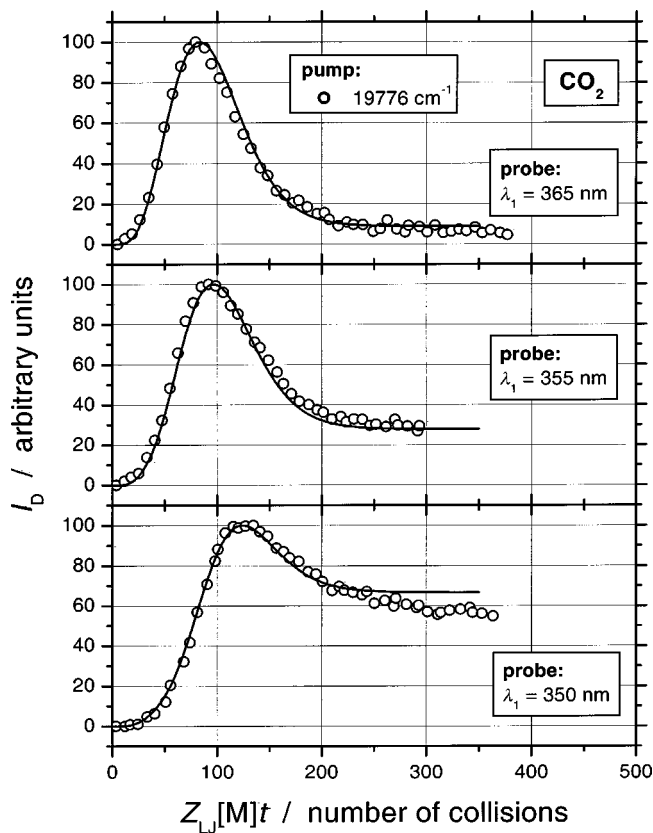
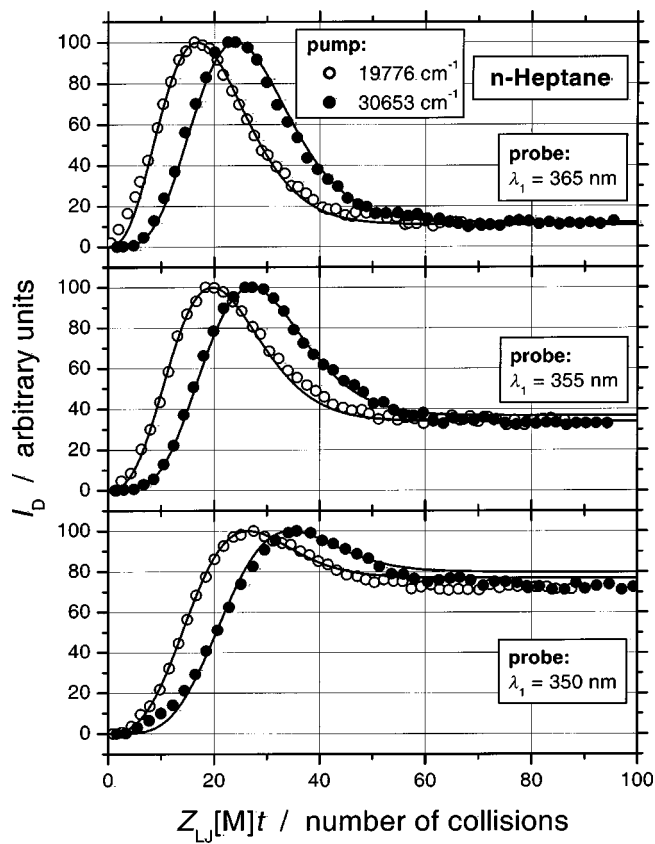FIG. 11. Same as in Fig. 10, but for the collider CO_2.

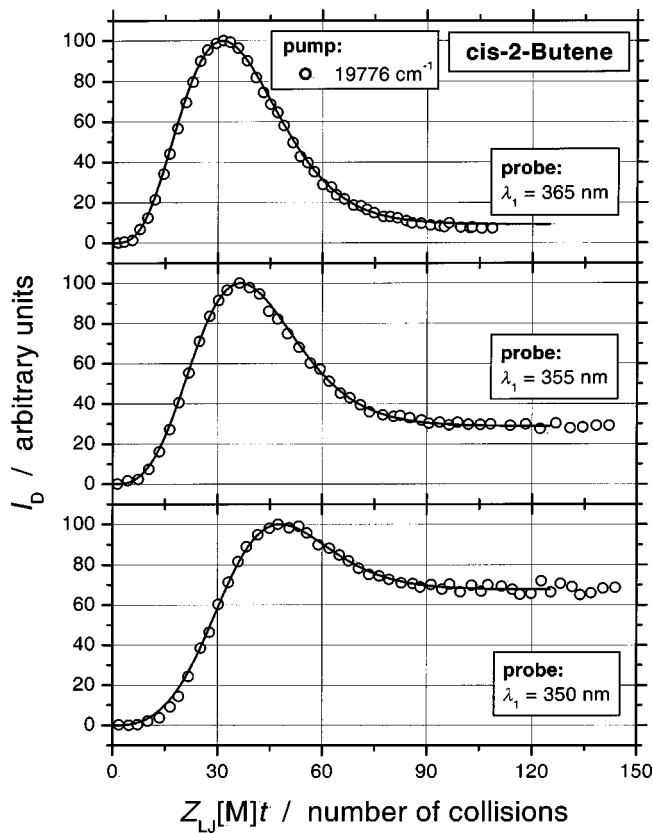FIG. 13. Same as in Fig. 7, but for the collider *n*-heptane.

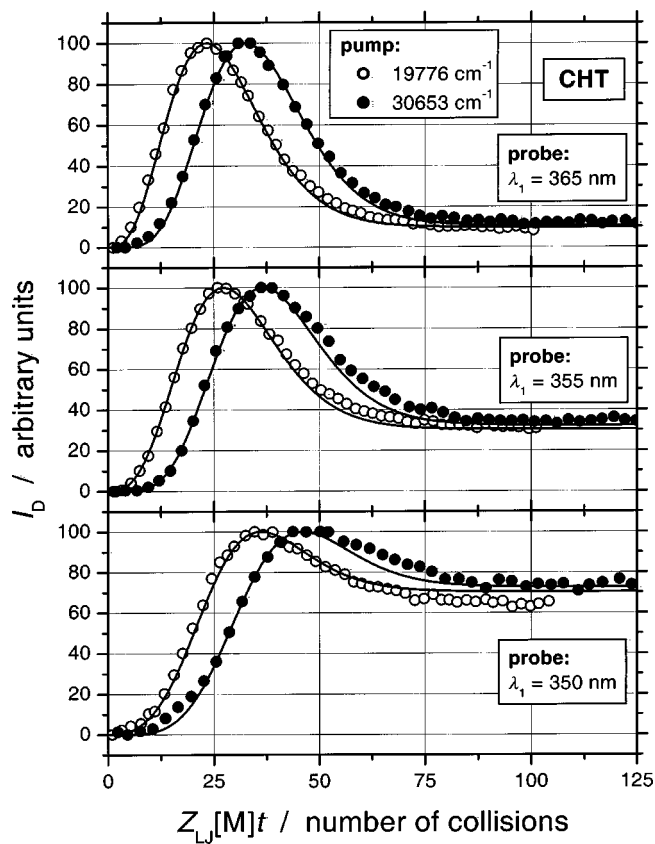FIG. 12. Same as in Fig. 10, but for the collider *cis*-2-butene.

FIG. 14. Same as in Fig. 7, but for the collider CHT.

TABLE IV. Optimized parameters for the monoexponential transition probability $P(E',E)$ with parametric exponent Y and energy dependent parameter $\alpha_1(E) = C_0 + C_1 \cdot E$ [see Eq. (16)].

Bath gas	C_0 (cm^{-1})	C_1 (10^{-3})	Y
He	28	2.30	0.65
Ar	33	4.20	0.65
Xe	28	4.50	0.65
N$_2$	50	6.00	0.70
CO$_2$	130	8.30	0.80
cis-2-butene	380	39.0	1.20
CHT	450	51.0	1.20
n-heptane	645	59.5	1.20

$$P(E',E) = \frac{1}{c(E)} \exp\left[-\left(\frac{E-E'}{\alpha_1(E)} \right)^Y \right]$$
$$= \frac{1}{c(E)} \exp\left[-\left(\frac{E-E'}{C_0+C_1E} \right)^Y \right], \quad (E' \leq E), \quad (16)$$

where $c(E)$ is a normalization constant. The upward branch of $P(E',E)$ with $E'>E$ is then given by detailed balance. The best fit master equation simulations using this functional
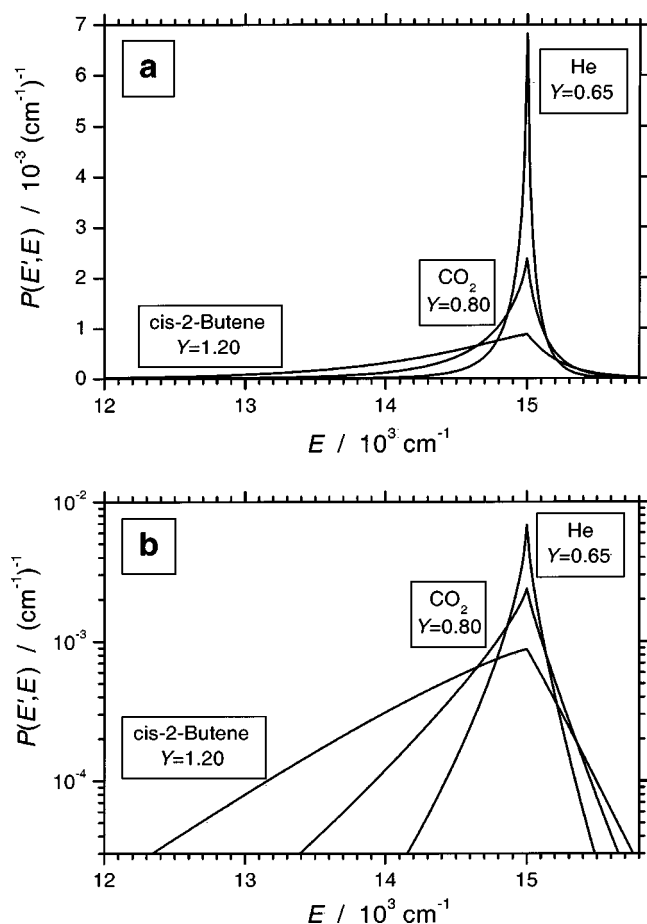

FIG. 15. (a) Linear representation of the monoexponential transition probabilities $P(E',E)$ with parametric exponent Y in the argument [Eq. (16)] for the bath gases helium, CO$_2$, and cis-2-butene at $E = 15\,000$ cm^{-1}; (b) same as in (a) but using a semilogarithmic representation. Note the *concave* overall curvature for $Y<1$ (helium and CO$_2$) and the *convex* curvature for $Y>1$ (cis-2-butene). The parameters are from Table IV.
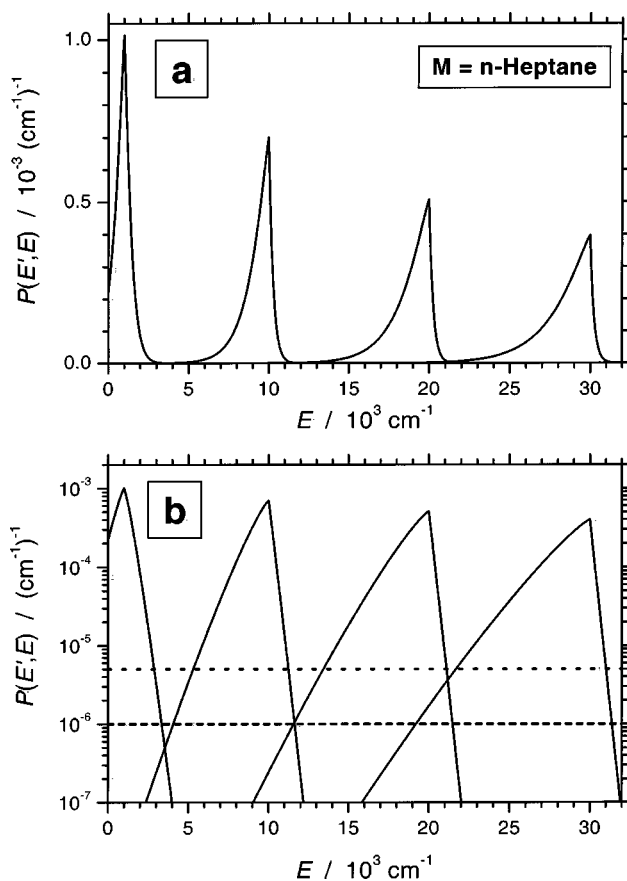

FIG. 16. Collisional transition probabilities $P(E',E)$ for the collider n-heptane at the excitation energies 1000, 10 000, 20 000, and 30 000 cm^{-1}. (a) Linear and (b) semilogarithmic representation. Note the "convex" shape in the lower plot ($Y=1.2$). The dotted horizontal line in (b) at $P(E',E)_d = 5 \times 10^{-6}$ (cm^{-1})$^{-1}$ shows the cut-off value for the simulations in Fig. 17. The dashed line at $P(E',E)_d = 1 \times 10^{-6}$ (cm^{-1})$^{-1}$ represents the cut-off value which would produce KCSI simulations indistinguishable from those employing the full $P(E',E)$.

are included in Figs. 7–14. Table IV shows the parameters for the whole set of colliders. There is a remarkably smooth and uniform increase of *all three parameters* (C_0, C_1, and Y) with the "size" of the collider. Y varies between 0.65 for helium and 1.2 for large polyatomics. For an illustration how the shape of $P(E',E)$ changes for selected bath gases with different Y values, see Fig. 15. In the semilogarithmic representation, exponents $Y<1$ correspond to a "concave" curvature, whereas exponents $Y>1$ yield a "convex" curvature. Compared with the linear shape of monoexponential $P(E',E)$ at $Y=1$, this clearly classifies only small colliders with $Y<1$ as having relatively enhanced probabilities for transfer of large ΔE. On the contrary, large colliders systematically show $Y>1$ and thus a *relative* drop-off of $P(E',E)$ in the wings or reduced probabilities of "supercollisions."

These findings are very similar to our recent KCSI results for toluene,[4] where parametric exponents Y between 0.65 (helium) and 1.5 (n-heptane) were found, as well as a linear energy dependence of the parameter $\alpha_1(E)$ for all colliders. It occurs as a general behavior in all the systems studied by the KCSI technique so far. Very recently, Nordholm et al. have presented an extension[14] of their partially ergodic collision theory (PECT).[46–48] This very simple and intuitive

statistical theory, which is of course no model on dynamical detail, is nevertheless the first one which can reproduce both the bath gas dependence of Y and the energy dependence of $\alpha_1(E)$ on a sometimes even quantitative level. It therefore appears as if Eq. (16)—originally proposed by us empirically as a very flexible $P(E',E)$ functional with a minimum number of parameters—also can be justified on the basis of a statistical description without dependence on detailed assumptions of very specific dynamics. This situation seems to indicate parallels with the success—and limitations—of statistical theories in reactive processes. A detailed discussion is given in the article following this one.

B. Influence of the long $P(E',E)$ tails on the energy flow

Considering recent debates on CET it is interesting to check, to which extent long tails of $P(E',E)$ distributions at large $|E'-E|$ have an influence on the energy transfer behavior and how they will appear in the shape of our KCSI simulations. Small changes in $P(E',E)$ will show up during the collision cascade as clear changes of the resulting $g(E)$ distributions, because the KCSI signal is very sensitive to cumulative effects. The following discussion is based on the heptane case, but it should be stressed at this point that any other collider, e.g., argon or CO_2, could have been taken, i.e., the findings are independent of the detailed curvature of $P(E',E)$, and are valid (within small numerical differences) for colliders with $Y<1$ and $Y>1$ alike. Additional examples are omitted here only for the sake of brevity.

The energy dependent shape of the heptane $P(E',E)$ is shown in Fig. 16 for the energies 1000, 10 000, 20 000, and 30 000 cm^{-1} in a linear (a) and semilogarithmic (b) representation. In the lower plot, one can clearly notice the convex shape of $P(E',E)$ for this bath gas ($Y=1.2$). In addition, the energy dependence of the parameter $\alpha_1 = C_0 + C_1 \cdot E$, which leads to an increase of the width of $P(E',E)$ with increasing energy, is evident in both plots. We carried out detailed master equation simulations, in which we took the optimized parameters from Table IV, but deliberately truncated $P(E',E)$ at a certain value, e.g., 5×10^{-6} (cm^{-1})$^{-1}$ [dotted line in Fig. 16(b)]. When doing so, the normalization constants $c(E)$ in Eq. (16) must be adjusted. Note that this is an approximate procedure which will—to a small extent—diminish the contribution of the tail, as the amplitude of the remaining part of the truncated $P(E',E)$ will be scaled up compared to its untruncated counterpart. The resulting $g(E)$ population distributions and corresponding KCSI simulations for an observation window at 355 nm are shown in Fig. 17 as dashed lines for the collider n-heptane. Solid lines correspond to simulations with the full $P(E',E)$. We see a minor difference for the truncated $P(E',E)$: As expected, the $g(E)$ distributions and KCSI simulations lag a bit behind those employing the full $P(E',E)$, due to the lack of a few efficient deactivating collisions. An analysis of runs for several cut-off parameters and a variety of bath gases shows that for values $\leq 1 \times 10^{-6}$ (cm^{-1})$^{-1}$ [dashed line in Fig. 16(a)] the simulations with full and truncated $P(E',E)$ become indistinguishable. A more detailed calculation including an exact treatment of the normalization procedure will lead to a decrease of this cut-off value, which however—as our preliminary calculations show—will not let this limit drop below 1×10^{-7} (cm^{-1})$^{-1}$.

The message from such an analysis is, that the influence of collisions in the $P(E',E)$ wing at amplitudes below roughly 1×10^{-6} (cm^{-1})$^{-1}$ is indeed negligible in the large majority of applications. For instance, in the typical kinetic competitions between unimolecular reactions and CET these collisions will not matter because of their very low statistical contribution. One exception to this will only be a clear single collision situation, like in special chemical activation systems, with conditions under which statistical chances of sequential collisional activation are so low that especially efficient single collisions are the only way to introduce at all a reaction with a high product activation barrier in a strongly deactivating solvent.
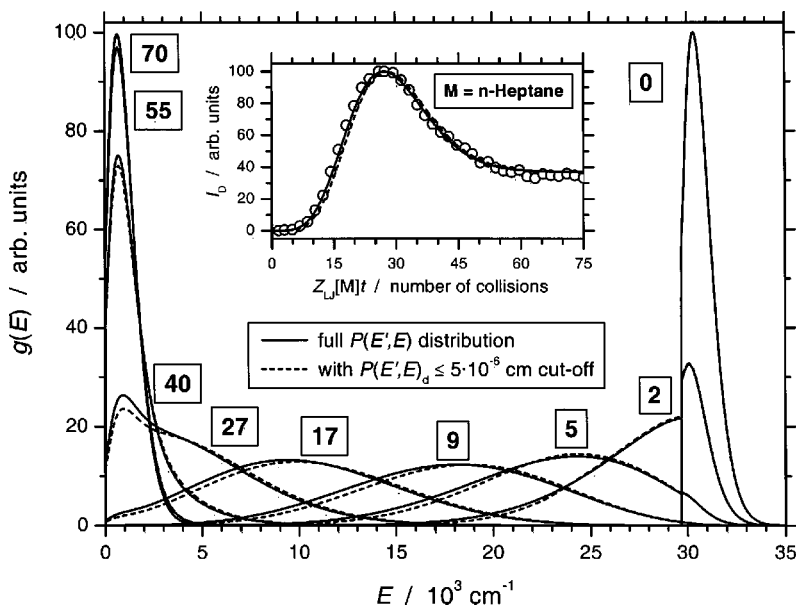

FIG. 17. Evolution of a population of highly vibrationally excited azulene molecules during a typical collisional relaxation process. Collider: n-heptane. Solid line: Master equation simulation employing the full $P(E',E)$. Dashed line: Same simulation, but with $P(E',E)_d$ amplitudes truncated for $\leq 5 \times 10^{-6}$ (cm^{-1})$^{-1}$. Each number corresponds to the number of collisions experienced for the respective distribution. The inset shows the KCSI curve and corresponding simulations at $\lambda_1 = 355$ nm.

J. Chem. Phys., Vol. 119, No. 21, 1 December 2003
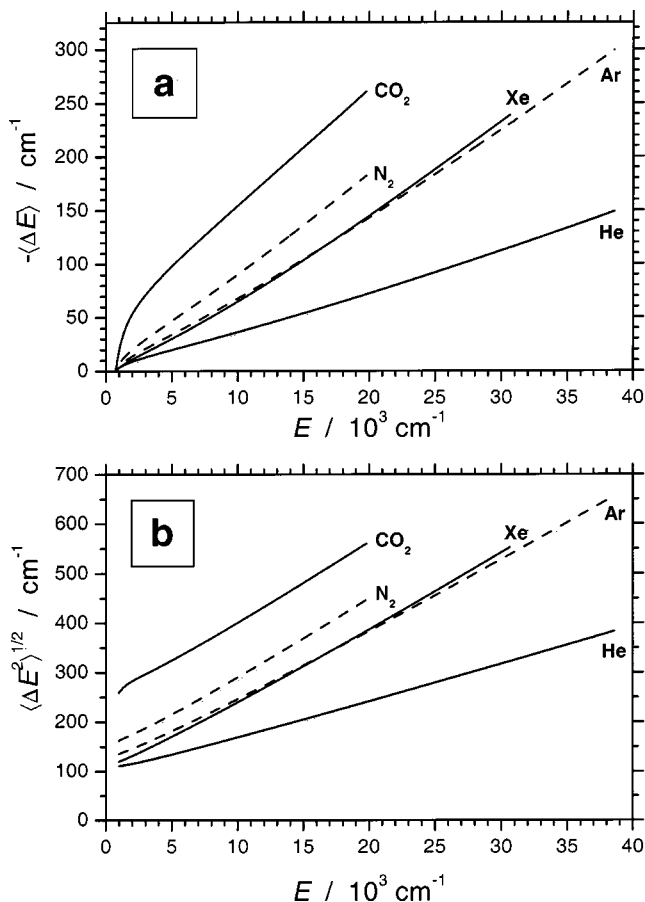
Energy transfer of highly excited molecules   11205

FIG. 18. (a) First moments of energy transfer $\langle\Delta E\rangle$ and (b) square roots of the second moment of energy transfer $\langle\Delta E^2\rangle^{1/2}$ as functions of energy for the colliders helium, argon, xenon, N_2, and CO_2. See also Tables V–VII.

FIG. 19. Same as in Fig. 18, but for the colliders *cis*-2-butene, CHT, and *n*-heptane.

C. Moments of energy transfer $\langle\Delta E^n\rangle$ for azulene from $P(E',E)$

Having established our optimized $P(E',E)$ parameters we can evaluate every energy transfer quantity of relevance. We are specifically interested in the energetic dependence of the moments of energy transfer,

$$\langle\Delta E(E)^n\rangle = \int_0^\infty (E'-E)^n P(E',E)dE', \qquad (17)$$

$n=1$ is denoted as the first moment, the average energy transferred per collision $\langle\Delta E\rangle$, which represents the sum over all downward (=deactivating) and upward (=activating) collisions. The second moment ($n=2$), the mean-squared energy transferred per collision $\langle\Delta E^2\rangle$, is related to the width of $P(E',E)$ and therefore also the width of the relaxing distribution $g(E,t)$.

$\langle\Delta E\rangle$ and the square root of the second moment, $\langle\Delta E^2\rangle^{1/2}$ are plotted in Figs. 18 and 19 for all bath gases, employing the optimized $P(E',E)$ parameters from Table IV. For the following discussion, the first and second moments are summarized for selected energies in Tables V and VI. In addition, Table VII contains the parameters of accurate third order polynomial fits to $\langle\Delta E\rangle$ and $\langle\Delta E^2\rangle^{1/2}$ for the energy range between roughly 4000 and 40 000 cm^{-1} and the bath gases of this study.
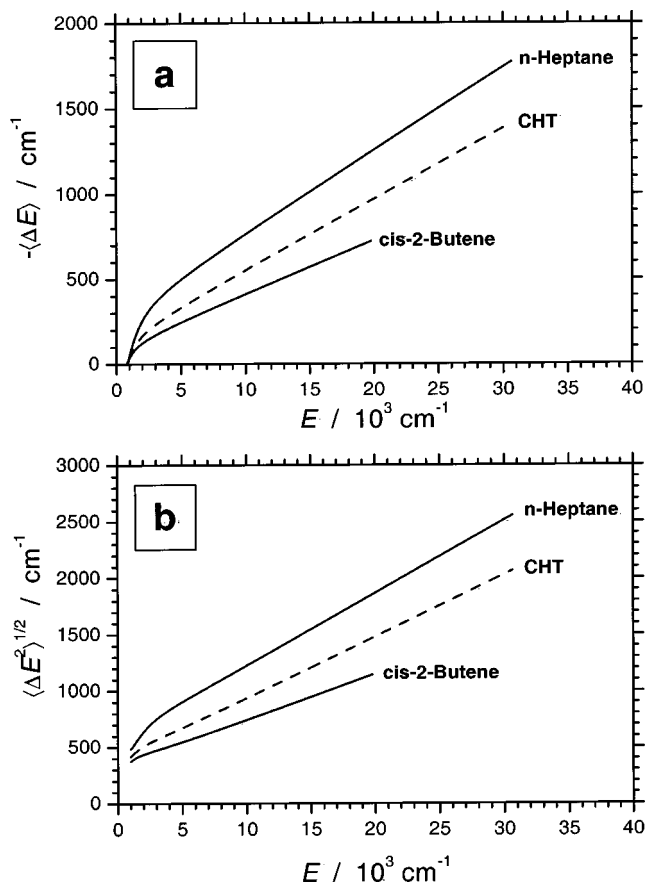
For all colliders, $\langle\Delta E(E)\rangle$, the average energy transferred per collision, is approximately linear, with the exception of the lowest energies ($E \leq 2000–5000\ cm^{-1}$, depending on the bath gas). $\langle\langle\Delta E\rangle\rangle = 0$ has to be fulfilled in thermal equilibrium ($\langle E\rangle = \langle E\rangle_{th}$), thus, the sudden turn towards zero energy transfer is due to the constraints of detailed balancing when approaching $\langle E\rangle_{th}$, here 300 K. A more detailed look at the first moments reveals a small upwards curvature of $-\langle\Delta E\rangle$ with increasing energy beyond the low range for small colliders up to N_2. However, this slightly concave shape disappears with increasing size of the polyatomic colliders. Interestingly, the "crossing" of the $\langle\Delta E\rangle$ curves for

TABLE V. $\langle\Delta E\rangle$ values calculated from $P(E',E)$ of KCSI. Parameters, see Table IV.

	$-\langle\Delta E\rangle$ (cm^{-1}) at						
Bath gas	5000 cm^{-1}	10 000 cm^{-1}	15 000 cm^{-1}	20 000 cm^{-1}	25 000 cm^{-1}	30 000 cm^{-1}	35 000 cm^{-1}
He	20	36	54	72	92	112	133
Ar	34	68	104	143	183	225	268
Xe	30	65	103	145	188	233	⋯
N_2	47	90	136	184	⋯	⋯	⋯
CO_2	98	154	208	263	⋯	⋯	⋯
cis-2-butene	245	410	570	728	⋯	⋯	⋯
CHT	331	550	761	969	1176	1382	⋯
n-heptane	497	763	1011	1255	1498	1739	⋯

TABLE VI. Same as in Table V, but for $\langle \Delta E^2 \rangle^{1/2}$.

Bath gas	$\langle \Delta E^2 \rangle^{1/2}$ (cm^{-1}) at						
	5000 cm^{-1}	10 000 cm^{-1}	15 000 cm^{-1}	20 000 cm^{-1}	25 000 cm^{-1}	30 000 cm^{-1}	35 000 cm^{-1}
He	134	169	205	242	279	317	356
Ar	182	246	314	384	455	528	602
Xe	170	240	312	387	464	542	⋯
N_2	215	290	369	450	⋯	⋯	⋯
CO_2	324	401	481	563	⋯	⋯	⋯
cis-2-butene	547	743	945	1152	⋯	⋯	⋯
CHT	673	936	1206	1479	1753	2029	⋯
n-heptane	903	1225	1546	1867	2190	2512	⋯

the bath gases argon and xenon in Fig. 18(a) at $E \approx 16\,700$ cm^{-1} is not only found in azulene, but was also observed in our earlier study on toluene, where it was, however, shifted to lower energies (about 8000 cm^{-1}).[4]

A statistical χ^2 error analysis was carried out to get upper and lower bounds for the parameters of the $P(E',E)$ expression in Eq. (16) (see also the discussion in the end of Sec. III B). This translates into an estimate for the uncertainties in our $\langle \Delta E(E) \rangle$ curves. Note that this method yields results, which are practically identical to those obtained from a "visual inspection" procedure, as discussed in our earlier publication.[4] We find very small errors in $\langle \Delta E \rangle$ of about 2%–5% over the whole deactivation range (about 40 000 cm^{-1} for helium and argon, 30 000 cm^{-1} for xenon, CHT and *n*-heptane, and 20 000 cm^{-1} for all other colliders). This is even smaller than in our toluene study (2%–7%), and underlines the high accuracy of the first moment data from KCSI experiments. The reason for this is easily understood: For excitation at 19 776 cm^{-1} we have "full KCSI visibility" of the $g(E)$ distributions, as the signal immediately rises after the beginning of the deactivation (Figs. 7–14). Curves for higher excitation energies (30 653 and 38 573 cm^{-1}) show a clearly defined period with "zero signal" before the actual rise of the KCSI signal. The difference in risetime of these signals compared to those starting at 19 776 cm^{-1} is a crucial experimental parameter: It is directly correlated with the absolute $\langle \Delta E \rangle$ at high energies and imposes very severe constraints on possible $\langle \Delta E(E) \rangle$ dependencies in the energy range above our direct "KCSI visibility" range.

The second moment of energy transfer, $\langle \Delta E^2 \rangle$, the mean-squared energy transferred per collision, also shows a pronounced energy dependence. The same order of increasing values for the various collider gases is found as for the first moments. This becomes more evident after removing the quadratic dependence, as done in the plots of Figs. 18(b) and 19(b): $\langle \Delta E^2 \rangle^{1/2}$, the square root of the second moment, also follows an approximately linear dependence on energy rather similar to that observed for all $\langle \Delta E \rangle$ curves. The same type of cross over in the order of collider efficiencies from argon>xenon at low energies to xenon>argon at high vibrational energies appears as in the first moments.

V. COMPARISON WITH RESULTS FROM OTHER EXPERIMENTS

A. KCSI experiments for toluene

We have recently published detailed experimental KCSI data for the collisional deactivation of toluene starting at an excitation energy of about 50 000 cm^{-1}.[4,49] The similarities between the $P(E',E)$ distributions from the toluene and azulene experiments were already discussed above.

It is standard practice in the literature to compare the first moments of different excited molecules for the same collider. Often then, $\langle \Delta E \rangle$ values and their energy dependences are discussed and interpreted, without considering differences in the collision numbers. In a majority of applications, e.g., in chemical reaction kinetics, the rates of energy transfer are the actual quantities of interest, typically in a competitive situation of CET with reactive or other processes. A comparison of the full rate coefficient of CET or related quantities is therefore much closer to actual needs, and also avoids any problems of the best choice and the energy dependence of collision numbers. For that reason, we consider the energy dependence of the moments $k_{E,n}$ of the rate coefficients $k(E',E)$ for CET given by

$$k_{E,n} = Z_{LJ} \langle \Delta E(E)^n \rangle. \tag{18}$$

Specifically, we are interested in a comparison of $k_{E,1}$, the first moment of the rate coefficient [in units of cm^3 s^{-1} times energy (here in cm^{-1})], as shown in Fig. 20.

There are two important findings. First, both excited molecules, toluene and azulene, show a similar linear in-

TABLE VII. Third order polynomial fits to the first and second moments of energy transfer for collisions between azulene and the collider M. Valid from 4000 cm^{-1} up to E_{max}, where $E_{max}=38\,573$ cm^{-1} (M=He, Ar), 30 653 cm^{-1} (Xe, CHT, *n*-heptane), or 19 776 cm^{-1} (N_2, CO_2, *cis*-2-butene). $\langle \Delta E \rangle = A_0 + A_1 \cdot E + A_2 \cdot E^2 + A_3 \cdot E^3$ and $\langle \Delta E^2 \rangle^{1/2} = A_0 + A_1 \cdot E + A_2 \cdot E^2 + A_3 \cdot E^3$ calculated using the transition probability $P(E',E)$ of Eq. (16) with the parameters from Table IV.

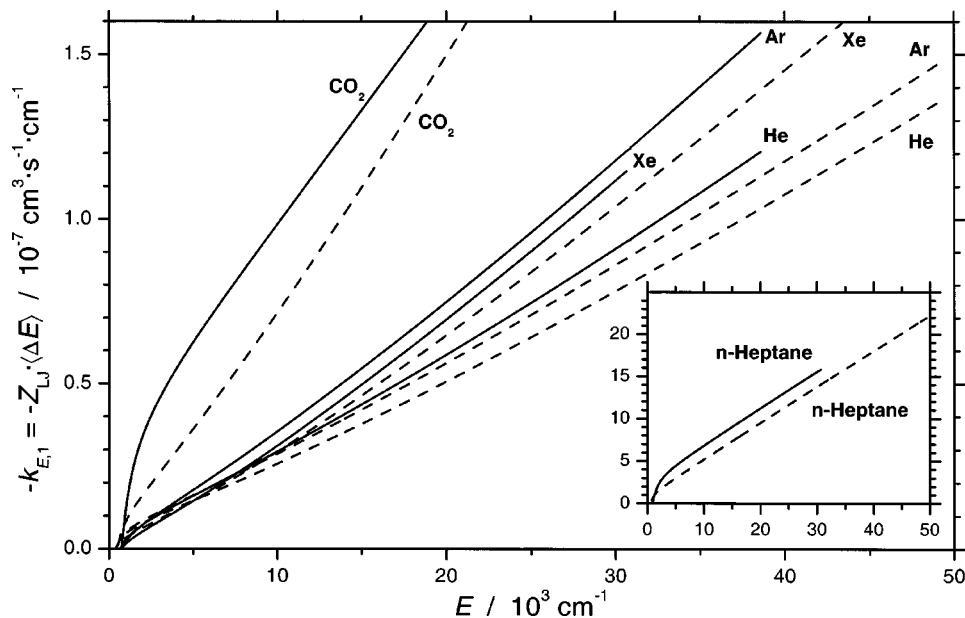| M	$\langle \Delta E \rangle$				$\langle \Delta E^2 \rangle^{1/2}$			
	A_0 (cm^{-1})	A_1 (10^{-3})	A_2 (10^{-8} cm)	A_3 (10^{-13} cm^2)	A_0 (cm^{-1})	A_1 (10^{-3})	A_2 (10^{-8} cm)	A_3 (10^{-13} cm^2)
He	−4.27	−2.97	−2.42	1.06	101.05	6.57	2.76	−2.09
Ar	−2.89	−5.89	−6.63	5.18	120.21	11.93	7.44	−6.26
Xe	0.29	−5.60	−10.36	10.37	104.96	12.71	8.54	−7.86
N_2	−5.16	−8.13	−3.44	−3.64	147.30	12.84	16.93	−27.50
CO_2	−32.10	−14.22	26.31	−65.35	256.12	12.73	20.98	−39.56
cis-2-butene	−59.87	−39.19	53.21	−122.89	368.14	33.99	42.80	−85.02
CHT	−97.17	−47.97	31.72	−49.06	417.88	49.93	21.63	−30.57
n-heptane	−200.61	−61.56	64.17	−100.55	566.76	67.40	−18.93	35.18

FIG. 20. Comparison of $k_{E,1}$, the first moment rate coefficients of CET, from KCSI measurements for azulene (solid line, this work) and toluene (dashed line, Ref. 4). Colliders: helium, argon, xenon, CO_2, and n-heptane (inset).

crease of $-k_{E,1}$ with energy. Second, for all colliders we find that azulene is more efficient than toluene. At this point—briefly coming back to a ''per collision'' picture—we note that this difference can be explained largely by the difference between the toluene and azulene collision numbers. The latter ones are consistently larger by 10%–20%. In the picture of individual molecular collisions in the gas phase one would therefore argue, that the larger Lennard-Jones diameter and well depth of azulene produces more inelastic collisions compared to toluene, and that the average energy transferred in a single collision for both systems is not so different. Still this cannot account for all the observed effects, e.g., for the colliders argon and n-heptane.

We ascribe this to the fact that azulene has more low lying vibrational frequencies compared to toluene and is therefore slightly more efficient. Trajectory calculations for large molecules by us[50] and others[51,52] as well as work on smaller systems[53–55] have shown that low frequency vibrations, especially those showing large amplitude motions, are the dominant gateway modes in large molecule CET under gas phase conditions. The idea itself dates back to the model of Landau and Teller,[56] which however is only valid for linear atom-diatomic collisions in the *adiabatic* limit ($\langle \Delta E \rangle \rightarrow 0$), so the applicability of such models to the large systems studied here, showing substantial amounts of inelastic collisions, is not necessarily expected.
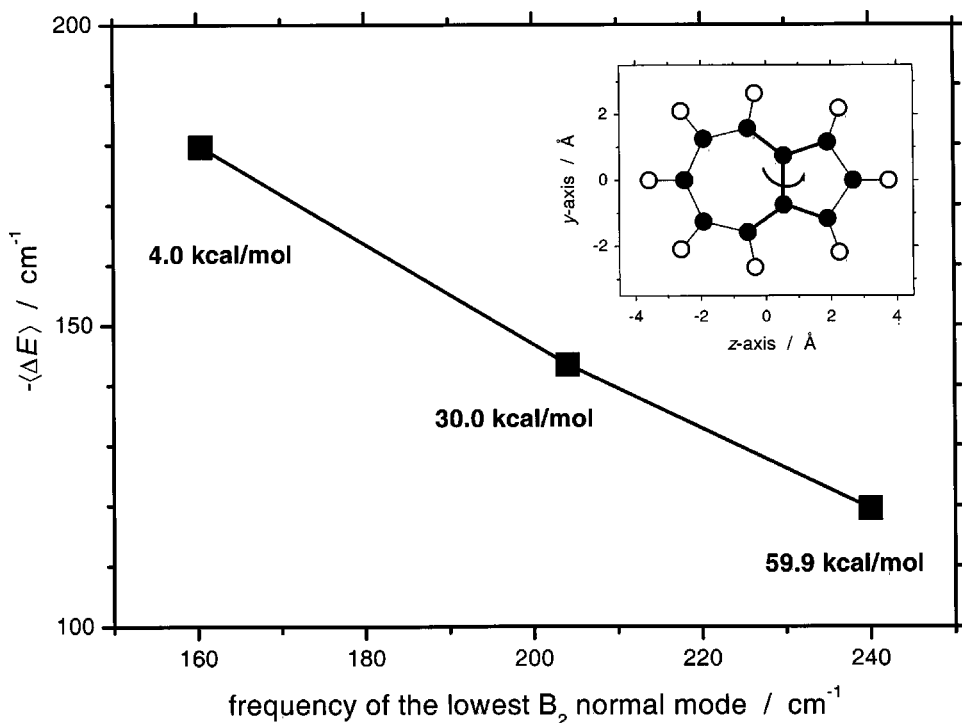

FIG. 21. Dependence of $\langle \Delta E \rangle$ on the frequency of the lowest B_2 normal mode of azulene as obtained from classical trajectory calculations for azulene*+argon. The frequency can be selectively tuned by adjusting the torsional barrier for the bond connecting the 5- and 7-membered rings. A smaller barrier corresponds to a reduced stiffness of the azulene skeleton allowing extended large amplitude out-of-plane motions of the ring structure.
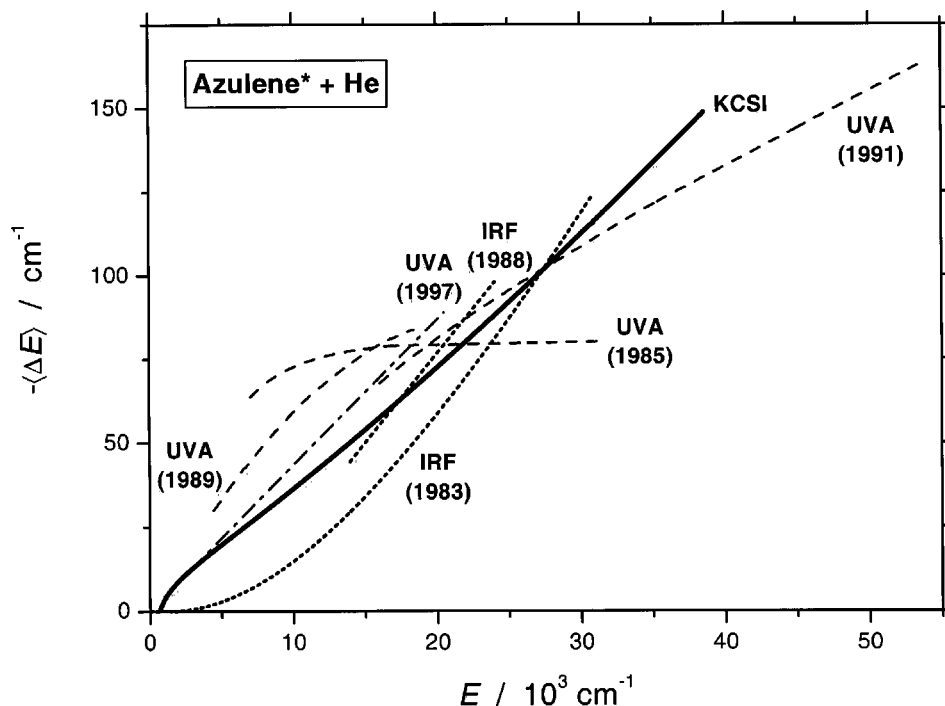
FIG. 22. KCSI energy dependence of $\langle\Delta E\rangle$ for azulene*+helium (solid line) compared with IRF results (dotted lines) from Ref. 6 (IRF 1983) and Ref. 9 (IRF 1988); UVA data (dashed lines) from Ref. 10 (UVA 1985), Ref. 11 (UVA 1989), Ref. 12 (UVA 1991), and UVA results (dashed–dotted lines) from Ref. 13 (UVA 1997). All curves are scaled to the collision number in Table II.

The impact of low frequency modes can be nicely illustrated by some of our accompanying trajectory calculations for azulene–Ar collisions (Fig. 21). For these, we used our valence force field (VFF) already successfully employed in a study of temperature dependent collisional energy transfer in the azulene system.[57] By changing the torsional barrier for twisting around the central C–C bond connecting the 7- and 5-membered rings, we can selectively tune the second lowest vibrational frequency of azulene (i.e., change the stiffness of the azulene ring system), and thereby study its influence on $\langle\Delta E\rangle$. Experimentally, this frequency has been determined as 240 cm^{-1},[36] corresponding to a torsional barrier of 59.9 kcal mol^{-1} in our best fit VFF. By artificially lowering the barrier down to 4 kcal mol^{-1} this frequency drops to about 160 cm^{-1}, which is accompanied by a jump in $-\langle\Delta E\rangle$ from 120 to 180 cm^{-1}. Obviously, the less stiff the ring, the more efficient CET.

B. "First moment" data from UVA and IRF experiments

Over the years, azulene has served as a benchmark system for studies of collisional energy transfer. The data most relevant for comparison with the KCSI measurements comes from time-resolved methods employing UV absorption and IR fluorescence spectroscopy. As these methods cannot provide transition probabilities $P(E',E)$, we will restrict the following discussion to a comparison of the energy dependence of the first moments $\langle\Delta E(E)\rangle$. Strictly speaking, UVA and IRF yield $\langle\!\langle\Delta E(\langle E\rangle)\rangle\!\rangle$, which corresponds to a $\langle\Delta E(E)\rangle$ "bulk averaged" over the distribution $g(E)$ having energy $\langle E\rangle$,

$$\langle\!\langle\Delta E(\langle E\rangle)\rangle\!\rangle = \int_0^\infty g_{\langle E\rangle}(E')\langle\Delta E(E')\rangle dE'. \tag{19}$$

However, we have already shown earlier that differences between the microcanonical and the respective bulk averaged values of the first moments are small, as long as one is sufficiently far away from thermal equilibrium.[4] In the following, we therefore use the notation $\langle\Delta E\rangle$ for both quantities and we have not transformed our KCSI $\langle\Delta E\rangle$ into the bulk quantity in any plot of this paper. A comparison for the bath gas helium is shown in Fig. 22. All curves are scaled to the KCSI Lennard-Jones collision numbers (Table II).

1. UVA experiments

Four sets of UVA data are available. The earliest measurements by Hippler *et al.* reported an almost energy independent $\langle\Delta E\rangle$ for all bath gases studied, except at the lowest energies.[10] However, later experiments of the same group with a better signal quality employing low[11] and high excitation energies[12] found a more or less linear energy dependence with a possible leveling-off at high energies. Figure 22 shows that especially at lower energies the older UVA data lie considerably higher than the KCSI values. This is a general trend observed for all the bath gases studied in those experiments.

In a more recent study by the Göttingen group a further improved signal to noise ratio was achieved.[13] These experiments were carried out at temperatures ⩾373 K for excitation energies <20 000 cm^{-1}. Almost monoexponential decays of the UVA signals were observed. Because the calibration curve in this region exhibits an essentially linear energy dependence, this results in a linear energy dependence of $\langle\Delta E\rangle$ over the whole energy range. For the whole set of colliders, these data show the closest agreement with the KCSI measurements.
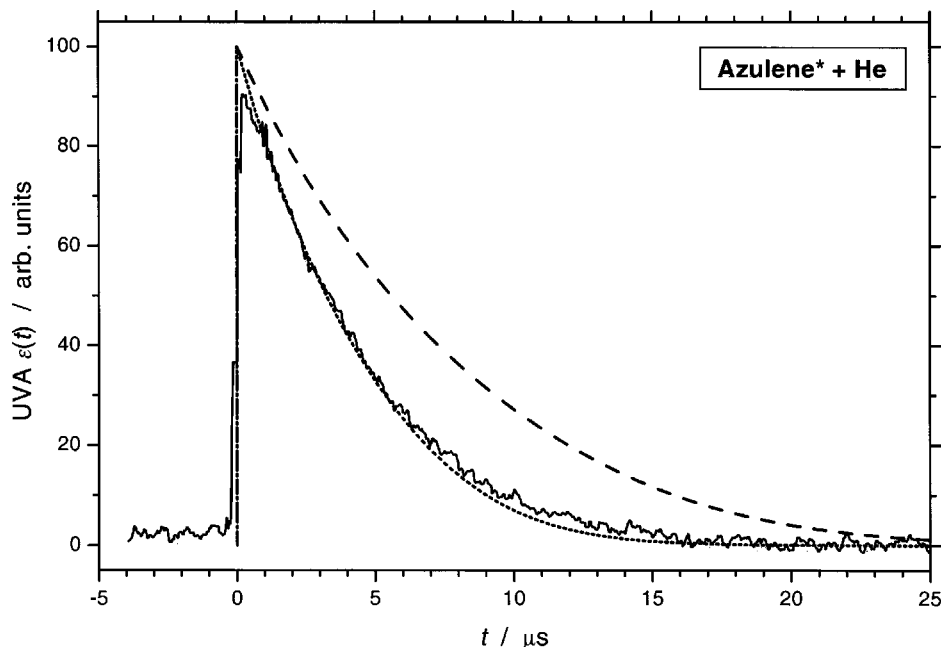
J. Chem. Phys., Vol. 119, No. 21, 1 December 2003

Energy transfer of highly excited molecules   11209

FIG. 23. Master equation simulations of experimental UVA data from Ref. 11 ($\lambda_{probe}=290$ nm, $T=298$ K) with $P(E',E)$ from KCSI. M=helium, $\lambda_0=590$ nm, $P_{total}=1592$ μbar, $P(\text{azulene})=9.89$ μbar, dashed line: fit using Eq. (16) and the $P(E',E)$ parameters for helium from Table IV, solid line: fit using Eq. (20) with parameters from Table IV for the first term (helium) and second term (CHT), as explained in the text; a fraction $x=P(\text{azulene})/P_{total}=9.89$ μbar/1592 μbar$=6\times10^{-3}$ was used to mimic a contribution of 0.6% azulene self-collisions. The calibration curve of Ref. 13 was used.

2. IRF experiments

The first time-resolved infrared fluorescence data for azulene were obtained by Barker and co-workers.[5,6] A later reanalysis by the same group with an "improved calibration curve" changed the original $\langle\Delta E\rangle$ values by 30%–50%.[9] In their so-called "simple analysis" they give values for two fixed energies ($\langle E\rangle=13\,943$ and $24\,023$ cm^{-1}). The results for helium are included in Fig. 22 and connected by dotted curves for the sake of clarity. Note that their argon results (not shown here) obtained from a more detailed master equation simulation in the same paper deviate substantially from the results of the "simple analysis." The IRF analysis predicts a linear increase of $-\langle\Delta E\rangle$ with excess energy as the KCSI data. However, the IRF moments deviate substantially, ranging from a different slope (Fig. 22) to a substantial overestimation of $-\langle\Delta E\rangle$ for other bath gases (not shown here).

3. Reanalysis and recommendation

For all colliders studied, a considerable spread of the $\langle\Delta E\rangle$ results is observed, as shown in Fig. 22 for the case of helium. Such diversity and spread of the literature data unfortunately support an existing and persisting belief among interested users of $\langle\Delta E\rangle$ data for chemical kinetics purposes, that the field of CET is still not really settled and taking some sort of average values from literature data corresponds to the state of the art. However, such a procedure is by no means advisable, as we have found out by confronting the available IRF and UVA data with the KCSI results.

We have analyzed all UVA and IRF data—as far as we had access to experimental traces—by calculating UV absorption profiles $\epsilon(t)$ and IR fluorescence intensity curves $I(t)$ from $g(E,t)$ of KCSI and the respective calibration curves $[\epsilon(\langle E\rangle)$ for UVA and $I(\langle E\rangle)$ for IRF, respectively].[9,13,58] Surprisingly, we can show very convincingly that all these measurements agree nearly perfectly with the $\langle\Delta E\rangle$ from KCSI, for azulene as well as toluene. Thus,

the problem of the—at first sight—puzzling differences among various "direct" values of $\langle\Delta E\rangle$ is solved. The detailed evidence will be published separately, tracing the observed differences back to either uncertainties in the IRF and UVA calibration curves[4,49] or influences of self-collisions, both leading to different deduced values of $\langle\Delta E\rangle$.[59]

For illustration, here we only give one example: In Fig. 23 a UVA trace for azulene*+helium is shown,[11] which decays much faster than the simulated fit (dashed curve) using the KCSI parameters from Table IV. A more detailed inspection of the experimental conditions reveals a non-negligible influence of azulene self-collisions in the UVA data sets. We tried to estimate the contribution of azulene–azulene collisions on the UVA trace by adding a second exponent to our $P(E',E)$ expression Eq. (16),

$$P(E',E)\propto\left\{(1-x)\cdot\exp\left[-\left(\frac{E-E'}{C_0+C_1\cdot E}\right)^{Y_1}\right]\right.$$
$$\left.+x\cdot\exp\left[-\left(\frac{E-E'}{B_0+B_1\cdot E}\right)^{Y_2}\right]\right\},\quad(E'\leq E).\quad(20)$$

Based on the experimental conditions given in Ref. 11 $[P(\text{azulene})/P_{total}=0.6\%]$ we took $x=6\cdot10^{-3}$ as a reasonable estimate for the contribution of efficient azulene–azulene collisions. Based on the $\langle\Delta E\rangle$ data in Ref. 9 one can extrapolate that the behavior of azulene as collision partner should be very close to that of CHT. Therefore, we used CHT parameters from Table IV for B_0, B_1, and Y_2 in the second exponent of Eq. (20). The resulting simulation (dotted curve) in Fig. 23 shows excellent agreement with the experimental trace and therefore strongly suggests a contamination of the UVA traces by self-collisions, which has not been considered in the extraction of the UVA $\langle\Delta E\rangle$ values.

A consistent set of such examples for several UVA and IRF signals will be given in our forthcoming publication.[59] By this procedure we can demonstrate that our "self-

calibrating'' KCSI data are in complete agreement with the body of available UVA and IRF measurements. Deviations in reported $\langle \Delta E \rangle$ values from UVA and IRF (as, e.g., in Fig. 22) must therefore be due to the following two systematic errors in the UVA and IRF experiments, namely (1) contributions of efficient azulene self-collisions which were not accounted for and (2) unavoidable uncertainties in the UVA and IRF calibration curves. The second point can have drastic effects, as we have already shown for toluene in part II of this series.[4]

On the basis of the present analysis one can give a clear recommendation: When available, KCSI data should be used, as they have the highest accuracy and can be—like in the present case—independent of any external calibration. Simply taking an average of several available measurements from different sources cannot be recommended in the light of the above discussion and the results of Ref. 59. Experiments using high fractions of the parent molecule should be checked for the contribution of self-collisions, and corrected accordingly. One should also analyze if calibration curves of sufficient accuracy were used, as this will possibly introduce a substantial source of error.

C. Trajectory calculations and theoretical models

Trajectory calculations have yielded a wealth of information on CET. In this respect, the pioneering work of Gilbert and co-workers for large systems, e.g., azulene+rare gases, has to be mentioned.[60] Due to computational limitations, only a few hundred trajectories were calculated in these early investigations, and first $\langle \Delta E \rangle$ values, most of them in the correct order of magnitude, could be obtained. Extended calculations by our group, using an improved valence force field for azulene, more sophisticated intermolecular potential functions and several 10 000 trajectories, reach an agreement within 30% of the experimental KCSI values.[57] Obtaining reliable $P(E',E)$ is an even more demanding task. Earlier calculations by us show that the intermolecular potential has an influence on the shape of the transition probability function.[61] Further calculations employing intermolecular potentials from *ab initio* calculations or molecular beam experiments will therefore be necessary to accurately model $P(E',E)$.

As far as theories are concerned, a complete model for describing details in large molecule energy transfer with predictive capabilities is still missing. One early approach was the ''biased randow walk (BRW)'' model by Gilbert which describes CET as a diffusive process in energy space using a Smoluchowski-type equation.[62] Systematic agreement was however not very convincing. In addition, the model predicts a shifted Gaussian form for $P(E',E)$, which is strongly at variance with each experimental $P(E',E)$ from KCSI in all systems studied so far.

On the other side, the large group of statistical models has to be mentioned.[63,64] Early simple approaches of this kind were hampered by the fact that they considerably overestimated the amount of energy transferred per collision, because they implicitly assumed a complete equilibration of all degrees of freedom in the collision complex. In reality, these collision complexes are, however, short-lived, as e.g., found

in trajectory calculations.[62] Therefore suitable modifications have to be introduced to account for incomplete redistribution of energy between the collision partners during their encounter. Very recently, a breakthrough in the statistical description of CET has been achieved. The ''partially ergodic collision theory (PECT)'' of Nordholm and co-workers[46–48] was extended by the same group to successfully predict the shape of the collisional transition probabilities in the toluene system.[14] A full account of the work for azulene is included in the following paper.[65] Here, we only want to mention that their modified statistical model represents the first theoretical approach which is able to qualitatively and semiquantitatively reproduce the shape of $P(E',E)$ from KCSI data. It therefore appears as if our—originally purely empirical—minimum parameter form of $P(E',E)$ [Eq. (16)] can thus be related to some basic physical background, as the overall mechanisms governing the energy transfer are apparently—to a considerable extent—correctly reproduced by a suitable statistical treatment.

VI. CONCLUSIONS

The collisional relaxation of highly vibrationally excited azulene in eight different bath gases has been studied using 2-color KCSI. A series of complete, experimental $P(E',E)$ distributions for this system could thus be obtained again, just as for toluene relaxation before.[4] All data could be represented perfectly by our recently proposed minimum parameter form for $P(E',E)$ with a variable exponent Y in the argument [Eq. (16)]. The systematic trends for various colliders found in our earlier studies on toluene were confirmed (from $Y<1$ for small monoatomic colliders to $Y>1$ for large polyatomic colliders). The different shapes of $P(E',E)$ can be explained by a modified statistical model which will be presented in the following paper.[65]

In approximate simulations we have quantified a nearly negligible influence of the wings of $P(E',E)$ at amplitudes roughly $<1\times10^{-6}(\text{cm}^{-1})^{-1}$ on the population distributions. Although further refined calculations will provide more detail, it is nevertheless already apparent that collisions at these low amplitudes are of negligible importance for the rates of chemical reactions, apart from rare special experimental situations. The $P(E',E)$ data reflect into moments $\langle \Delta E \rangle$ and $\langle \Delta E^2 \rangle^{1/2}$ of very high precision. A benchmark character of the data is achieved in this system as it is shown, that the results are ''self-calibrating.'' An experimental situation is reached, where no input of external molecular data (''calibration'' or ''reference'') is necessary, in contrast to all other available methods in energy transfer, like UVA and IRF. An (approximately) linear dependence of $\langle \Delta E \rangle$ and $\langle \Delta E^2 \rangle^{1/2}$ was found. Our study could even trace back systematic reasons for apparent deviations from the present results in earlier IRF and UVA studies on the CET of azulene. Contributions of azulene self-collisions were identified as a second effect in addition to the well-known large consequences of slight uncertainties in calibration curves.

[1] H. Hippler and J. Troe, in *Bimolecular Collisions*, edited by J. E. Baggott and M. N. R. Ashfold (The Royal Society of Chemistry, London, 1989), p. 209.

[2] I. Oref and D. C. Tardy, Chem. Rev. **90**, 1407 (1990).

[3] U. Hold, T. Lenzer, K. Luther, K. Reihs, and A. C. Symonds, J. Chem. Phys. **112**, 4076 (2000).

[4] T. Lenzer, K. Luther, K. Reihs, and A. C. Symonds, J. Chem. Phys. **112**, 4090 (2000).

[5] M. J. Rossi and J. R. Barker, Chem. Phys. Lett. **85**, 21 (1982).

[6] M. J. Rossi, J. R. Pladziewicz, and J. R. Barker, J. Chem. Phys. **78**, 6695 (1983).

[7] J. R. Barker, J. Phys. Chem. **88**, 11 (1984).

[8] J. R. Barker and R. E. Golden, J. Phys. Chem. **88**, 1012 (1984).

[9] J. Shi and J. R. Barker, J. Chem. Phys. **88**, 6219 (1988).

[10] H. Hippler, L. Lindemann, and J. Troe, J. Chem. Phys. **83**, 3906 (1985).

[11] H. Hippler, B. Otto, and J. Troe, Ber. Bunsenges. Phys. Chem. **93**, 428 (1989).

[12] M. Damm, F. Deckert, H. Hippler, and J. Troe, J. Phys. Chem. **95**, 2005 (1991).

[13] C. Hanisch, diploma thesis, University of Göttingen, 1997.

[14] D. Nilsson and S. Nordholm, J. Chem. Phys. **116**, 7040 (2002).

[15] D. Schwarzer (unpublished).

[16] A. A. Ruth, E.-K. Kim, and A. Hese, Phys. Chem. Chem. Phys. **1**, 5121 (1999).

[17] L. Rupp, Ph.D. thesis, University of Göttingen, 2001.

[18] M. Fujii, T. Ebata, N. Mikami, and M. Ito, Chem. Phys. **77**, 191 (1983).

[19] J. W. Lewis, R. V. Nauman, D. B. Bouler, Jr., and S. P. McGlynn, J. Phys. Chem. **87**, 3611 (1983).

[20] E. W. Thulstrup, P. L. Case, and J. Michl, Chem. Phys. **6**, 410 (1974).

[21] W. Gerhartz and J. Michl, J. Am. Chem. Soc. **100**, 6877 (1978).

[22] A. Amirav and J. Jortner, J. Chem. Phys. **81**, 4200 (1984).

[23] T. Suzuki and M. Ito, J. Phys. Chem. **91**, 3537 (1987).

[24] S. K. Kulkarni and J. E. Kenny, J. Chem. Phys. **89**, 4441 (1988).

[25] H.-J. Kray and B. Nickel, Chem. Phys. **53**, 235 (1980).

[26] D. Huppert, J. Jortner, and P. M. Rentzepis, J. Chem. Phys. **56**, 4826 (1972).

[27] T. M. Woudenberg, S. K. Kulkarni, and J. E. Kenny, J. Chem. Phys. **89**, 2789 (1988).

[28] O. K. Abou-Zied, D. R. M. Demmer, S. C. Wallace, and R. P. Steer, Chem. Phys. Lett. **266**, 75 (1997).

[29] M. Votsmeier, Ph.D. thesis, University of Göttingen, 1995.

[30] Y. Hirata and E. C. Lim, J. Chem. Phys. **69**, 3292 (1978).

[31] The fluorescence quantum yields for energies up to 15 000 cm^{-1} above the S_2 origin were kindly provided by Professor A. Amirav (1992).

[32] M. Damm, H. Hippler, and J. Troe, J. Chem. Phys. **88**, 3564 (1988).

[33] R. Fröchtenicht, H.-G. Rubahn, and J. P. Toennies, Chem. Phys. Lett. **162**, 269 (1989).

[34] L. Brouwer and J. Troe, Int. J. Chem. Kinet. **20**, 379 (1988).

[35] L. Brouwer, H. Hippler, L. Lindemann, and J. Troe, J. Phys. Chem. **89**, 4608 (1985).

[36] R. S. Chao and R. K. Khanna, Spectrochim. Acta, Part A **33A**, 53 (1977).

[37] D. Tanaka, S. Sato, and K. Kimura, Chem. Phys. **239**, 437 (1998).

[38] M. Klöppel-Riech, Ph.D. thesis, University of Göttingen, 2000.

[39] A. Amirav and J. Jortner, Chem. Phys. Lett. **95**, 295 (1983).

[40] J. A. Syage, P. M. Felker, and A. H. Zewail, J. Chem. Phys. **81**, 4685 (1984).

[41] T. S. Zwier, E. Carrasquillo, and D. H. Levy, J. Chem. Phys. **78**, 5493 (1983).

[42] J. Troe, J. Phys. Chem. **87**, 1800 (1983).

[43] A. C. Symonds, Ph.D. thesis, University of Göttingen, 1992.

[44] S. H. Fishtine, Z. Phys. Chem., Neue Folge **123**, 39 (1980).

[45] U. Hold, T. Lenzer, K. Luther, K. Reihs, and A. C. Symonds, Ber. Bunsenges. Phys. Chem. **101**, 552 (1997).

[46] L. Ming, T. D. Sewell, and S. Nordholm, Chem. Phys. **199**, 83 (1995).

[47] L. Ming, J. Davidsson, and S. Nordholm, Chem. Phys. **201**, 121 (1995).

[48] L. Ming, J. Davidsson, and S. Nordholm, J. Chem. Phys. **104**, 9001 (1996).

[49] U. Grigoleit, T. Lenzer, K. Luther, M. Mützel, and A. Takahara, Phys. Chem. Chem. Phys. **3**, 2191 (2001).

[50] T. Lenzer, K. Luther, J. Troe, R. G. Gilbert, and K. F. Lim, J. Chem. Phys. **103**, 626 (1995).

[51] C. Heidelbach, J. Schroeder, D. Schwarzer, and V. S. Vikhrenko, Chem. Phys. Lett. **291**, 333 (1998).

[52] D. C. Clary, R. G. Gilbert, V. Bernshtein, and I. Oref, Faraday Discuss. **102**, 423 (1995).

[53] H. Hippler, H. W. Schranz, and J. Troe, J. Phys. Chem. **90**, 6158 (1986).

[54] H. W. Schranz and J. Troe, J. Phys. Chem. **90**, 6168 (1986).

[55] G. Lendvay, J. Phys. Chem. A **101**, 9217 (1997).

[56] L. D. Landau and E. A. Teller, Phys. Z. Sowjetunion **10**, 34 (1936).

[57] U. Grigoleit, T. Lenzer, and K. Luther, Z. Phys. Chem. (Munich) **214**, 1065 (2000).

[58] J. Shi, D. Bernfeld, and J. R. Barker, J. Chem. Phys. **88**, 6211 (1988).

[59] T. Lenzer and K. Luther, Phys. Chem. (to be published).

[60] K. F. Lim and R. G. Gilbert, J. Phys. Chem. **94**, 77 (1990).

[61] T. Lenzer and K. Luther, J. Chem. Phys. **105**, 10 944 (1996).

[62] R. G. Gilbert, J. Chem. Phys. **80**, 5501 (1984).

[63] Y. S. Lin and B. S. Rabinovitch, J. Phys. Chem. **74**, 3151 (1970).

[64] J. Troe, Ber. Bunsenges. Phys. Chem. **77**, 665 (1973).

[65] D. Nilsson and S. Nordholm, J. Chem. Phys. **119**, 11212 (2003), following paper.